UNIVERSITÀ DI PARMA

UNIVERSITA' DEGLI STUDI DI PARMA

DOTTORATO DI RICERCA IN

FISICA

CICLO XXXII

Optical characterization of structure and dynamics from single droplets to emulsions

Coordinatore:
Prof. Stefano Carretta

Tutor:
Prof. Luigi Cristofolini
Prof. Libero Liggieri

Dottoranda: Fabrizia Salerni

Anni 2016/2019

TABLE OF CONTENTS

ABBREVIATIONS

APD	Avalanche photodiode
CMC	Critical Micellar Concentration
DLS	Dynamic Light Scattering
DWS	Diffusing Wave Spectroscopy
EDDI	Emulsion Dynamics and Droplet Interface *A research project funded by ESA aiming to investigate emulsions under aging in microgravity condition using the SMD facility.*
ESA	European Space Agency
ISS	International Space Station
MCT	Medium Chain Trigliceride *Edible oil composed of glycerides of medium chain fatty acid.*
SDS	Sodium Dodecyl Sulfate *Model surfactant widely used in industry consisting of a 12-carbon tail attached to a sulfate group.*
SMD	Soft Matter Dynamics *Facility onboard the Columbus modulus of the ISS, devoted to the study of soft matter dynamics based on the optical technique of DWS.*

ABSTRACT

Aim of the present research is to investigate the intimate link between the properties of the single droplet interface and the mechanisms involved in emulsion formation and stability. Emulsion stability is a subject of enormous technological relevance, with potential impact over different types of industries (pharmaceutical, foods, petrochemical, cosmetics, and more). In particular, the target is to optimize the amount of additives used in order to reduce the potential negative impact and production costs, and to replace ionic with non-ionic surfactants for benefits to the environment and human health.

Emulsions are dispersions of immiscible liquids in which one is dispersed in the other in form of droplets. Surfactants are molecules that, when adsorbed at the liquid-liquid interface, facilitate emulsion production and promote its stability. Stability is related to dynamic properties of the adsorbed layer. Under specific conditions, the stability of this layer contrasts droplets aggregation and coalescence that could cause droplet to growth and phase separation. Interfacial dilational viscoelasticity, namely interfacial tension response to droplets area variation, is of considerable importance against coalescence. Destabilization processes and emulsions evolution have been studied at different scales, from microscopic to macroscopic, by a combination of different optical techniques: microscopy and macro imaging, digital images elaboration, interfacial tensiometry and Diffusing Wave Spectroscopy (DWS). DWS is a non invasive optical technique based on the temporal analysis of coherent light scattered inside a turbid system, such as an emulsion. The technique detects the internal dynamic of the emulsion and allows to obtain an indirect measurement of structural (droplet mean size) and rheological (mechanical modulus) features. In this work, the long-term stability of a paradigmatic alkane in water emulsion stabilized by sodium dodecyl sulfate (SDS) at concentration well below the Critical Micellar Concentration (CMC) has been characterized. The most important result concerns the internal dynamic of emulsion in the long-time regime, explained also in terms of elementary process at the droplets interface. The aging of stable emulsions shows a slowing down of the dynamics, presumably related to progressive drainage of water and to the slowly increase of drop packing, as the value of average droplet radius estimated remains constant. At constant aging, the dynamics shows a peak of the relaxation time as a function of surfactant concentration. This implies that the bulk shear mechanical modulus shows a maximum; this maximum corresponds to an analogous maximum found in the dilational modulus of the single interface by drop tensiometry.

1. EMULSIONS: MORPHOLOGY, STABILITY AND DYNAMICS

1.1 INTRODUCTION AND MOTIVATIONS

A vast number of natural and synthetic products are emulsions: from food to cosmetics, pharma, housekeeping products and more.

Emulsions are defined as metastable dispersions of one liquid in another in the form of droplets whose size ranges from nanometers up to micrometers and more. Emulsions can be classified according to the nature of their continuous phase as:

- oil-in-water, if oil droplets are dispersed in a continuous aqueous phase;
- water-in-oil, if water droplets are dispersed in a continuous oil phase.

Except for microemulsions, which are outside of the present study, emulsions are thermodynamically unstable. Therefore, the tendency of the two liquids to minimize the interfacial area favours droplets aggregation until the complete separation of the two liquid phases.

In order to form emulsions:

- energy must be applied to the mixture of immiscible or mutually insoluble liquids. The amount of energy is related to an increase of the interfacial area obtained dispersing one phase in the other; initially the interface between the two phases is deformed by forming large droplets that subsequently broken up into smaller ones;
- surface-active species (surfactants, polymers, proteins, particles and their mixture) facilitate emulsification. They adsorb at the liquid-liquid interface decreasing the energy needed for the creation of new area (interfacial tension) and modify suitably the chemico-physical and mechanical features of the interface, contrasting destabilization mechanisms.

An example of oil-in-water emulsion obtained with addition of surfactant an its adsorption at droplet surface is sketched in Figure 1.

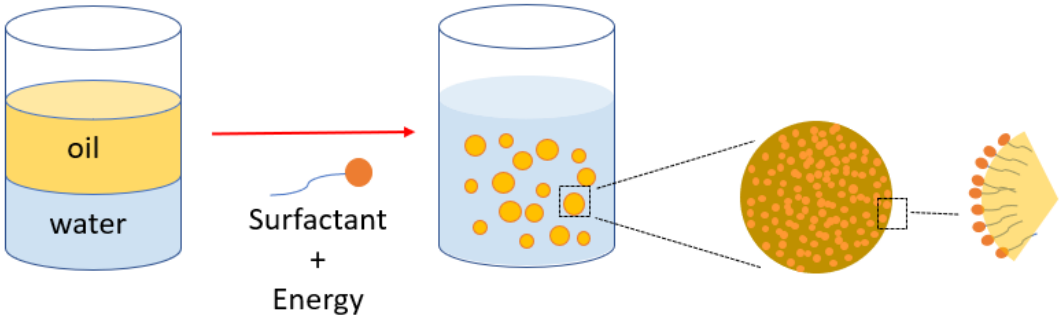

Figure 1 Sketch of the processes concurring to obtain an emulsion.

Satisfactory emulsification and stable emulsions are achieved when a uniform distribution of small droplets of the dispersed phase are created and phase separation slows down. Droplet size distribution and evolution depend on the surface-active characteristics and on the molecular adsorption at the interface. Emulsions with micrometric droplets and different densities of the constituting liquids show phase separation due to gravity. Dispersed droplets less dense than the dispersing fluid tend to rise to the surface (to cream), denser droplets in contrast tend to sediment. If size of the droplets is nanometric, their random thermal motion may be overcome by the gravitational force [1].

This research is motivated by applicative and environment/ecological interests, in particular targets on the amount of surface-active emulsifier that is often not fully optimized in qualitative and quantitative terms. Furthermore, gravity imposes limits in the emulsion formation and subsequent destabilization (drainage of liquids). The effects of single processes on destabilisation mechanisms are hindered by creaming and/or sedimentation and the comprehension of emulsion hydrodynamics remains still challenging.

The research is linked to the project EDDI (Emulsion Dynamics and Droplet Interface) under ESA (European Space Agency) contract. By providing experiments in microgravity the aim is to understand the role of surfactants in emulsion production and stability in order to reduce and optimize the amount of emulsifiers utilized. The experiments will be executed onboard the Columbus modulus of the International Space Station (ISS) in the Fluid Science Laboratory where a dedicated facility, "Soft Matter Dynamics" (SMD) has been implemented. SMD is devoted to the study of soft matter dynamics and has been developed based on the optical technique of Diffusing Wave Spectroscopy (DWS). DWS is able to investigate dynamical and structural features of emulsions by detecting temporal interference speckles of coherent light

multiply scattered inside the sample. The embedding of the experiments on emulsion aging to be performed under weightless with a combination of macro and micro imaging, interfacial tensiometry and spectroscopic techniques on ground will provide data on specific processes in emulsions destabilisation. Based on the suppression of droplet buoyancy, it is expected that the destabilisation of the emulsion slows down, since drops are brought to interact only under the effect of capillary-driven or Brownian motion.

Microgravity condition allows to:

- develop and test all the mechanisms underlying the stability related to droplet dynamics influenced by surfactant layers and liquid features, such as adsorption dynamics and droplet coalescence and aggregation;
- investigate single events (coalescence or aggregation) and dynamic regimes.
- identify the conditions for the onset and the role of specific dynamic regimes under the sole effect of capillary-related features.

Results will be useful to develop and validate predictive models, as well as to check the existing ones. The present study reports the results used to address the design of the instrumental diagnostics suitable for the microgravity studies.

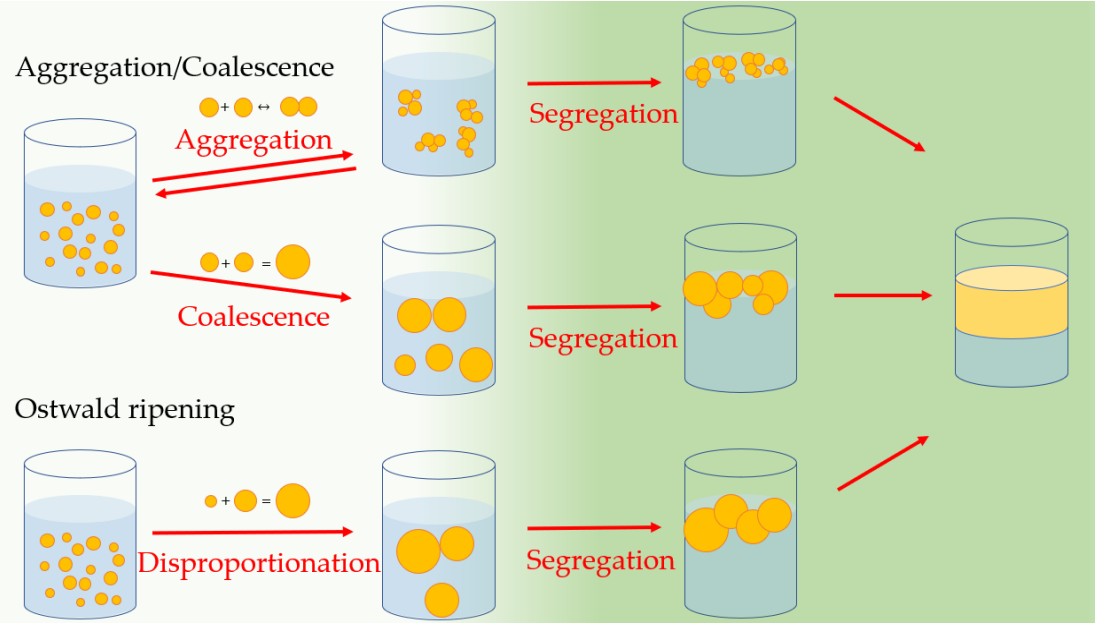

Figure 2 Sketch of the mechanisms involved in emulsion destabilization both in microgravity and on ground (white background) and only on ground (green background).

As sketched in Figure 2, emulsion destabilization involves different mechanisms that increase the average droplet size (coarsening) and therefore gravity sedimentation or creaming:

- Aggregation of droplets under the effect of inter-droplet interactions, which depends on the liquids, the surface-active molecules and the status of interface;
- Coalescence of small interacting droplets caused by the rupture of the thinning film of the matrix liquid between them [2];
- Ostwald ripening [3], [4], larger droplets grow at the expenses of the smaller ones driven by the Laplace pressure difference between them.

Emulsification and stability depend on the addition and the type of emulsifiers, the density and viscosity of the continuous phase, the droplet size distribution, the oil/water ratio, the temperature, the intensity of mechanical agitation and its duration. To realize a stable emulsion, it is important to analyse the connection between destabilization processes and the physical properties at the interface. A complete characterization of the properties of such complex system often requires a combination of different experimental techniques. This work reports on a study of the factors influencing emulsification, emulsion stability and aging, with the aim to provide perspectives to control emulsion properties.

Research is often devoted to evaluating different type of emulsification technique and achieving a stable drop size distribution using minimal amounts of surfactant. An investigation is reported in [5].

Emulsification efficiency depends on how the provided interfacial film between the two liquids minimizes their contact, coalescence and aggregation. In [6] the interaction between hydrophobic components of the surfactant and oil chain length is studied to provide insights on how it influences emulsion stability. It was observed a more rigid interface when the oil molecules increase penetration and their cohesion with the aliphatic layer of the surfactant film.
Furthermore, in [7] the influence of surfactant concentration is investigated. There is a concentration window out of which the volume of emulsion decreases because of the agglomeration of oil droplets (low concentration) or coalescence phenomena (high concentration). In [5] it is demonstrated that exists an emulsion fraction value, function of oil to water ratio, at which emulsion is best densely packed and remain constant over long period.
Several investigations show that the mean size of droplets decreases by increasing the intensity of emulsification and the duration of the process. For each emulsion there is

an optimum time of emulsification: as this time increases the emulsification becomes more effective, however beyond an optimum time the quality improves only a little because the emulsifiers may drop out from the oil-water interface [8].
Temperature effects emulsification: both interfacial tension and viscosity decrease for higher values, and there is an optimum emulsifying temperature influencing emulsifier adsorption [5].

In Chapter 3 results on emulsion stability are reported: it is affected by surfactant content, oil/water volume ratio, emulsification time and, even more dramatically, by emulsification processes.

1.2 SURFACTANTS

Surfactants are amphiphilic compounds containing both hydrophilic and hydrophobic groups. Schematically they are represented by a hydrophilic head linked at a hydrophobic tail composed by a long-chain of hydrocarbon groups. The polar head group may be anionic, cationic, non-ionic and zwitterionic; the tail of alkyl groups may be linear or branched. In this thesis the anionic surfactant used is a synthetic organic compound, sodium dodecyl sulfate (SDS), with 12 carbon chains attached to a sulfate group; it is highly water soluble. Non-ionic surfactants carry no net electrical charge; their water solubility derives from the interaction of their polar groups with water. Solubility depends on the different partitioning properties of hydrophobic and hydrophilic chains described by the partition coefficient, k_p , between water and oil. Oil and aqueous surfactant solution at known concentration c_{w0} and volumes, V_o and V_w respectively, are kept in contact for a long period to obtain the partition equilibrium. By using the method described in Section 2.1, the concentration of the surfactant in the aqueous depleted solution c_w is evaluated and the partition coefficient is calculated:

$$k_p = \frac{V_w}{V_o}\left(\frac{c_{w0}}{c_w} - 1\right). \quad (1)$$

Lower values of k_p implies that less amount of materials is needed, and it is possible to have a better control of the concentration in water.

The hydrophobic group determines the family name of the non-ionic surfactant, e.g. polyol esters, polyoxyethylene esters.

Adsorption at oil-water interface increases by adding surfactants in the phase where they are dissolved. For each surfactant a concentration characteristic, namely critical

micellar concentration (CMC), represents the limit of solubility of the molecules in the forms of monomers, which start to self-aggregate in solution to form micelles. Above the CMC, any surfactant addition increases the amount of micelles, while the concentration of monomers remains constant, as also the surface tension. Thus, as shown in Figure 3, the addition of surfactant at the solution decreases the surface tension as a function of surface coverage until the CMC is reached and surfactants start to form micelles in the bulk.

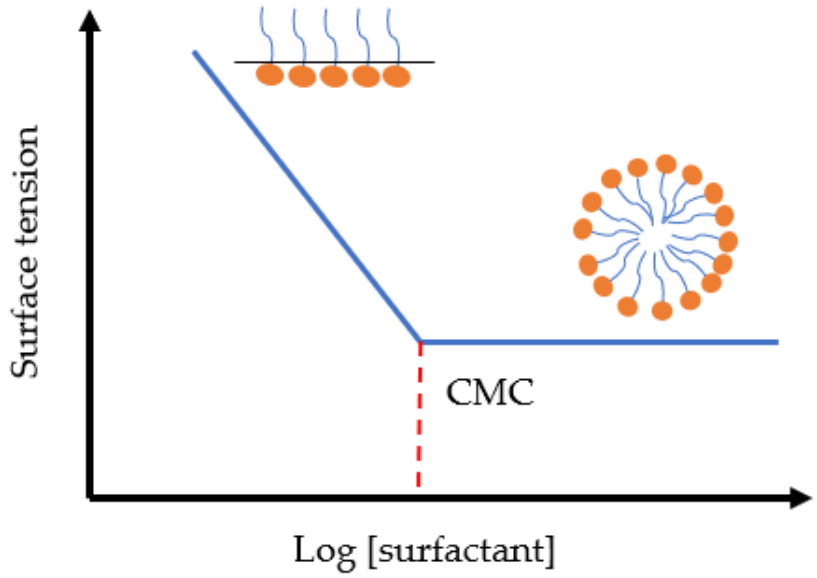

Figure 3 Surface tension versus surfactant concentration. At low concentration the surfactant is dissolved in the form of monomers able to adsorb at the interface, decreasing the surface tension. When the CMC is reached, the concentration of monomers remains constant, as also the surface tension.

2. METHODS

The work starts from the characterization of the surface properties of surfactants, via a complex analysis of the layer at water-air and water-oil interface (Section 2.1), and then moves to the study of real emulsions. Aging of emulsion is studied with complementary experimental approaches: macroscopic and microscopic imaging to understand emulsions structure and stability, and DWS for the investigation of internal dynamic as well as structure features. The theoretical backgrounds and a description of the used setups are reported in Sections 2.2, 2.3 and 2.4.

2.1 DROP SHAPE TENSIOMETRY: SINGLE INTERFACE

The study of the chemico-physical properties of the adsorption layer at water-oil interfaces such as dynamic interfacial tension and dilational viscoelasticity, is a mandatory step in modelling of aggregation and coalescence mechanisms in emulsions [9]. The aims are

- to characterize the chemico-physical and mechanical features of liquid-liquid interfaces, such as adsorption dynamics and dilational rheology, measuring the concerned quantities (dynamic/equilibrium interfacial tension, adsorption isotherm, adsorption kinetics, dilational viscoelasticity, partition coefficient etc.) on a large dynamic range;
- to develop models for the above features, accounting for the dynamic and structural aspects of adsorption layers. Depending on the system, surfactant exchange between the liquid phases may occur, which also need to be investigated and incorporated in the models.

For the compounds utilized dynamics behaviour of surface-active molecules at water/air and water/oil interfaces is investigated.

2.1.1 THEORETICAL BACKGROUND

The drop profile tensiometry determines interfacial tension (either for liquid-liquid or liquid-vapor interfaces) based on the shape of a drop deformed by gravity. Measurements require mechanical equilibrium of the interface to investigate adsorption kinetics at slow variations of the surface area or interfacial rheology at low frequency.

The shape of the drop at fixed volume tends to minimize the total energy of the system by balancing surface forces that make the drop spherical and gravity that vertically elongate or squeeze it. Interfacial tension can be calculated by fitting the theoretical profile of an axis-symmetric drops [10]–[13]. The latter is derived by the condition of mechanical equilibrium. In fact, at equilibrium, the curvature at a generic point P (see Figure 4) of the interface adjusts in a way that capillary pressure equilibrates the hydrostatic pressure. Following [13] that can be expressed in a set of three differential equations, known as the Brashfort-Adams equations [14], in terms of the chemico-physical parameters of the drop and of the coordinate of the drop profile

$$\frac{d\phi}{d\tilde{s}} = 2 \pm \beta\tilde{z} - \frac{sin\phi}{\tilde{x}} \tag{2}$$

$$\frac{d\tilde{x}}{d\tilde{s}} = cos\phi \tag{3}$$

$$\frac{d\tilde{z}}{d\tilde{s}} = sin\phi \tag{4}$$

where $\tilde{s}$ is the arc length, $\tilde{x}$ and $\tilde{z}$ are the horizontal and vertical coordinates of a point P of the profile (see Figure 4) respectively, normalized by the curvature radius at the drop apex b, ϕ is the angle of the polar angle of the point P and β the dimensionless shape factor. The latter relates drop deformation due to gravity acceleration g to the interfacial tension γ

$$\beta = \frac{\Delta\rho g b^2}{\gamma} \tag{5}$$

with $\Delta\rho$ density difference. The interfacial tension γ is evaluated by determining β from the best-fit of the calculated profile and the measured coordinates.

The oscillating drop method is also used to measure the dilational viscoelasticity E versus frequency by imposing a periodic drop area perturbation. Expansion or contraction of surface area causes dilational stress at the adsorbed layer, that is proportional to the relative area variation (purely elastic) and/or to the rate of surface

deformation (viscous) in presence of relaxation processes at the adsorbed layer. After adsorption equilibrium achievement, the interfacial tension response to sinusoidal perturbations of frequency ν is measured to obtain the complex dilation viscoelasticity

$$E = \frac{\Delta\gamma}{\Delta A/A_0} e^{i\varphi} . \tag{6}$$

The real and imaginary part of E are related to the dilational elasticity and viscosity respectively. The parameters of the signals (amplitude of oscillating surface tension $\Delta\gamma$ and area ΔA, and phase shift φ) are extracted by Fourier analysis at each frequency υ. Drop shape tensiometry is suitable for dilational viscoelasticity in a range spanning the decades between $10^{-5} - 10^{-1} Hz$. The upper limit being imposed by the need of preserving the mechanical equilibrium during the area oscillation. Dilational elastic character of the droplet surface is an important mechanical property in the study of droplet stability. Higher elasticity may tend to hinder the thinning of the thin film between two droplets making them more stable [15].

This technique is applicable to liquid-vapour or liquid-liquid interfaces using a small amount of the liquids. It is suitable for long time scale to follow slow process and broad frequency range in the mechanical equilibrium condition.

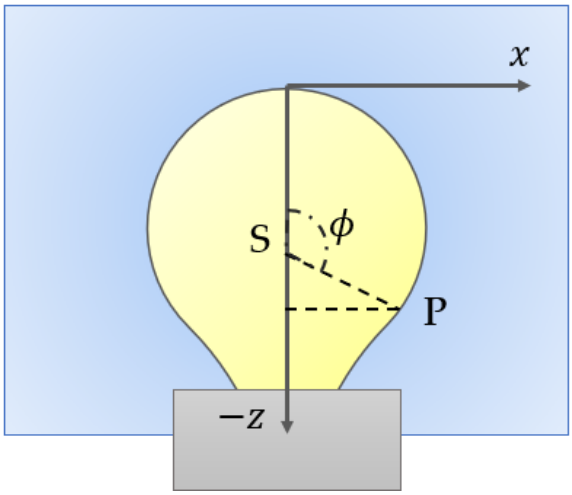

Figure 4 Sketch of the drop profile and (x, z) coordinate system for the emerging drop configuration.

2.1.2 SETUP

This Section reports the descriptions of the Drop Shape Tensiometry experimental arrangement assembled in the Laboratory ICMATE-CNR in Genova. As sketched in Figure 5 a drop is formed at the tip of a capillary immersed in another fluid inside a cell connected with a capillary tube to a micro-syringe pump (Hamilton, Switzerland) for drop volume dosage. Concerning the densities of the two phases there are two configurations, pendant and emerging drops, with vertical or of a U-shaped capillary respectively. A camera continuously acquires drop profile whose coordinates, obtained by image processing, are used to calculate surface tension by numerical fitting procedure. Experiments have been performed with PAT-1 model tensiometer (Sinterface Technologies, Berlin) [16] equipped with a CCD camera. The camera is coupled to a computer continuously monitors droplet images that are directly processed to calculate surface tension. A feed-back loop comparing observed droplet area and volume with the previous value is implemented, either to keep the droplet area constant or to impose automatic area variation cycles, in dependence of the type of measurement to be performed. Interfacial tension is measured with an accuracy of $0.1\,\frac{mN}{m}$ and minimum sampling time of $0.3\ s$.

Accuracy is influenced by calibration errors, in particular the determination of the ratio between orthogonal coordinates for the meridian drop-section is required for the conversion of CCD-camera-pixel unit to the length unit. Errors due to drop image distortion are usually negligible provided the drop size $\sim 4\ \mu m$.

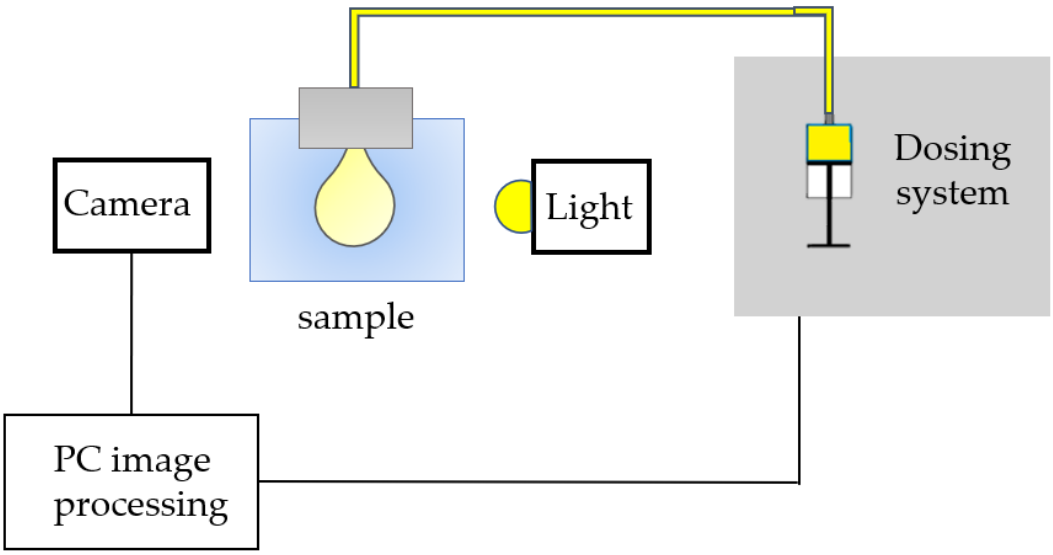

Figure 5 Sketch of the Drop Shape Tensiometry setup with control of the droplet profile coordinates.

2.2 IMAGING: EMULSION STABILITY

Temporal evolution of the emulsion volume with respect to the total volume of the liquids used is evaluated by macro imaging. The samples are held in glass vials or quartz cuvettes. A camera acquires pictures after the preparation. In this work we used an USB CCD camera (The Imaging Source DBK 31BU03 with resolution $1042x768\ pixels$ and frame rate $> 30\ fps$) equipped with a fixed focal objective with adjustable lenses and a manual iris (Cosmicar TV Lens $16mm$ and $f/1.4$). Pictures are taken at varying time intervals to follow emulsions aging. Images are calibrated against a standard and sequences are analysed by a Matlab script. The progress of the emulsion volume fraction $f_r = h_{em}/h_{total}$ is evaluated by measuring the relative heights h_{em}, h_{water} and h_{oil} of emulsion, water and oil phase respectively.

Figure 6 shows a representation of image acquisition and analysis. Emulsion evolution is depicted from the sequence of the sketch. The values of f_r are computed and illustrated in percentage as function of emulsion aging.

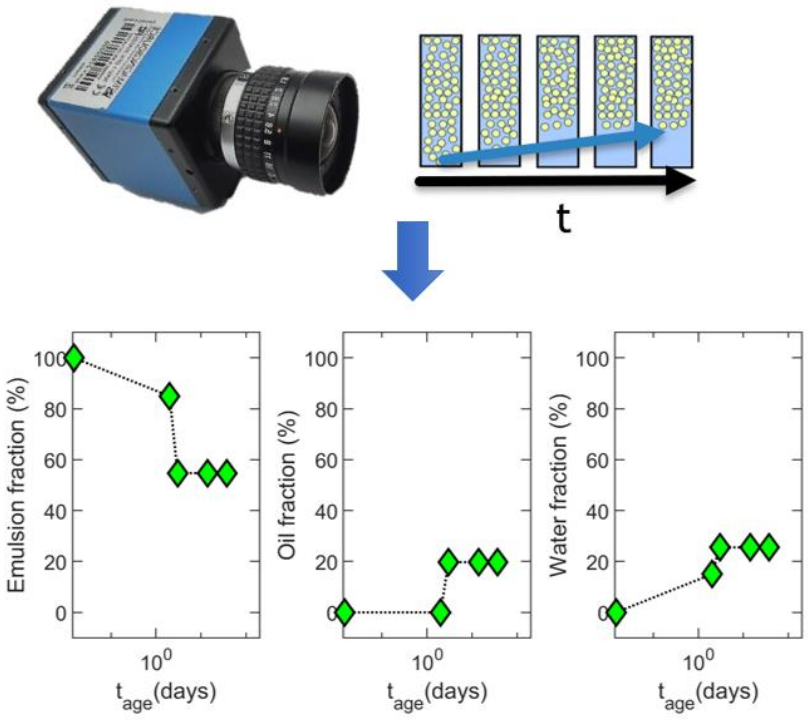

Figure 6 Scheme of the imaging setup and analysis. Top) the camera used at the University of Parma to follow emulsion aging by recording pictures and sketch of the effect of creaming and/or sedimentation; bottom) an example of emulsion, oil and water volume fraction as function of time.

2.3 MICROSCOPY: EMULSION MORPHOLOGY

Optical microscopy is used to accurately determine droplets size distribution by digital images processing. In this, it is assumed that the population of droplets adjacent at the wall is representative of the global population. This cannot be ascertained a priori and must be verified by comparing the size distribution obtained by microscopy with that obtained by other techniques sensitive to the bulk, such as DWS. Figure 7 shows a schematic of the analysis performed using a microscopy pointing directly to a lateral side of the quartz cuvette at a high of 1 cm from the top of the emulsion. In this work an optical microscope (Axiotech, Carl Zeiss) was used. It is equipped with objective, polarizers, dark and bright field, differential Interface contrast (DIC)) and a USB CCD camera (The Imaging Source DBK 31BU03 with resolution $1042x768\ pixels$ and frame rate $> 30\ fps$). Samples have been observed with Olympus ULWD50 long focal $50x$ objective (N.A. 0.55). Microscopy images have been analysed via ImageJ to evaluate droplet size distribution from a large number of droplets (~ 100). Droplets radius has been computed in pixel and converted in μm by a calibrating factor obtained by imaging of a calibration ruler with 100 μm spacing.

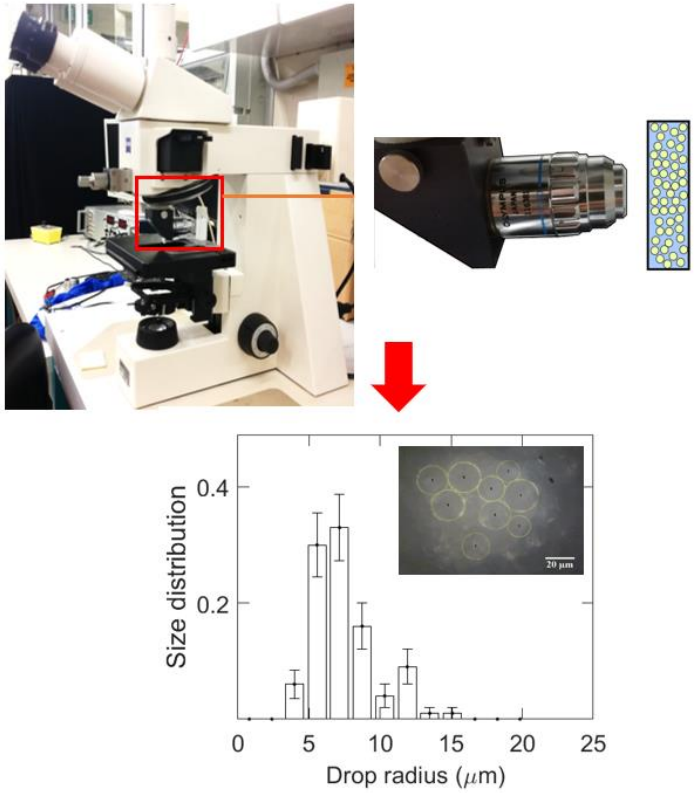

Figure 7 Scheme of the microscopy images acquisition and analysis. Top) Microscope used at University of Parma with objective pointing at the cuvette wall; bottom) an example of histogram of drop radius distribution obtained by droplets manual selection.

2.4 DIFFUSING WAVE SPECTROSCOPY: EMULSION DYNAMICS AND MORPHOLOGY

Diffusing Wave Spectroscopy (DWS) is an optical correlation spectroscopy used to investigate structure, dynamics and rheological properties of highly scattering samples and of interface-dominated systems, such as foams, emulsions or double emulsions [17]–[23]. Being based on optical detection of fluctuation intrinsic to the sample, DWS accesses at internal dynamics as well as to "scattering weighted" drop size mean value over the bulk in case of emulsion. It is a non-invasive method with a simple and robust experimental setup. For this reason, DWS has been selected as a diagnostic tool for emulsions investigation in microgravity. Moreover, being sensible to tiny motions and to fast time scales DWS extends the limits of usual microscopic, rheological and particle tracking techniques applied to turbid samples. Theoretical concepts are revised in Section 2.4.1. In Section 2.4.3 the setups used for experiments reported in that manuscript are described.

2.4.1 THEORETICAL BACKGROUND

DWS investigates sample dynamics by calculating temporal autocorrelation function $g_2(\tau)$ of coherent light intensity I detected after it has been multiply scattered within the sample

$$g_2(\tau) = \frac{\langle I(t)I(t+\tau)\rangle}{\langle I^2 \rangle} \quad . \tag{7}$$

The brackets $\langle ... \rangle$ corresponds to an average over time at a single point or over different speckles at the same time (multispeckle analysis). In both cases the speckle pattern results from the interference of light coming from different paths with a different number of scattering events and different lengths. A multispeckle acquisition accesses a slower time scale but has the advantage to reach good statistics in a short time (details in Section 2.4.2)[24].

Under the Gaussian approximation [25] each photon is considered to scatter a large number of time.

Then the intensity correlation function $g_2(\tau)$ is related to the electric field E correlation function $g_1(\tau) = \frac{\langle E^*(t)E(t+\tau)\rangle}{\langle |E|^2 \rangle}$ by the Siegert relation

$$g_2(\tau) = 1 + \beta |g_1(\tau)|^2 \tag{8}$$

where $\beta \leq 1$ is the contrast depending on instrumental factors of the experimental setup.

DWS links sample structure and dynamics to temporal fluctuations of the speckle pattern. Assuming light propagation as a diffusive process, photon phat is considered following a random walk in the sample. In a classical random walk each step of length equal to the mean free path l randomizes the direction of the walker. In an emulsion, given the size of the droplets being comparable with wavelength λ, scatters diffuse light preferentially in the forward direction and randomization requires a higher number of steps. This is described by the transport mean free path l^*[26], which is larger than l. In the light scattering processes of interest l^* is introduced to define the length over which direction of propagation is effectively randomized. This parameter is linked to the distance between scattering centres l and to the average scattering angle θ by the relation

$$l^* = l\frac{1}{\langle 1 - cos\theta \rangle} \tag{9}$$

in which $\langle 1 - \cos\theta \rangle$ measures the forward biasing.

In the case of emulsion in which droplets are compacted (high internal phase emulsions), it is known from numerical simulations [27] that l^* is proportional to the average drop size r. The relationship is obtained by a ray tracing algorithm based on Fresnel and Snell laws that simulates light propagation and scattering in a random packing of identical spheres [28], [29]. The proportional factor depends on the mismatch m of refractive index between dispersed and continuous phases and on packing fraction, resulting from a phenomenologically interpolation:

$$r = (-0.33782 + 0.34122\, m - 0.01368\, m^2) \cdot l^* . \tag{10}$$

One way of seeing DWS is to understand $g_1(\tau)$ as the sum of several correlations $g_{1,s}(\tau)$ each of one due to a single path of length s. These contribute to the total correlation function according to their statistical weight $P(s)$

$$g_1(\tau) = \int_0^\infty P(s) g_{1,s}(\tau) ds . \tag{11}$$

Being due to a single path length, $g_{1,s}(\tau)$ is a simple exponential decaying according to a quantity proportional to the mean square displacement of each scattering centre $\langle \Delta r^2(\tau) \rangle$ scaled by s/l^*, i.e. by the number of scattering events inherent to the path length s

$$g_{1,s}(\tau) = exp\left(-\frac{1}{3}\frac{s}{l^*}k_0^2\langle\Delta r^2(\tau)\rangle\right). \quad (12)$$

Longer paths decay faster due to the larger number of contributions. This helps to understand the different shape of the correlation functions obtained when measuring DWS in different geometries [30].

Of relevance in the present study are:

- Transmission (T): diffused light collected on the opposite side of illumination has minimum path length equal to the sample thickness L, meaning a faster decay of $g_2(\tau)$ due to longer paths contribution;
- Backscattering (B): diffused light collected on the same side of the illumination probes a wider distribution of path lengths, leading to a slower decay and a more stretched form of $g_2(\tau)$.

From a planar wave of incident light on the front face of the sample of thickness $L \gg l^*$, Backscattering and Transmission correlation functions are given by the formula

$$g_{2,B}(\tau) = 1 + \beta e^{-2\gamma\sqrt{\frac{6\tau}{\tau_0}}} \quad (13)$$

$$g_{2,T}(\tau) = 1 + \beta\left(\frac{\sqrt{\frac{6\tau}{\tau_T}}}{sinh\left(\sqrt{\frac{6\tau}{\tau_T}}\right)}\right)^2 \quad (14)$$

where τ_0 is the typical relaxation time for the fluctuation dynamic of the system and γ is a numerical factor. The role of this factor is to take into account short path in Backscattering, therefore with $\gamma = z_0/l^* + 2/3$ it is assumed that light originates from an arbitrary depth z_0 of the order of l^* inside the sample. It is experimentally observed [31] to vary between 1.5 and 2.7, depending on the size of particles and the setting of the polarization scheme of the measurement [32].
Backscattering correlation functions decays with τ_0, while Transmission decays with $\tau_T = \frac{1}{N}\cdot\tau_0$ that is faster due to the number of scattering events $N = \left(\frac{L}{l^*}\right)^2$.
Direct comparison of $g_{2,B}(\tau)$ and $g_{2,T}(\tau)$ allows to evaluate

$$l^* = \frac{L}{\sqrt{\tau_0/\tau_T}} \quad (15)$$

which is related to the structural average features of the sample from Equation 10.

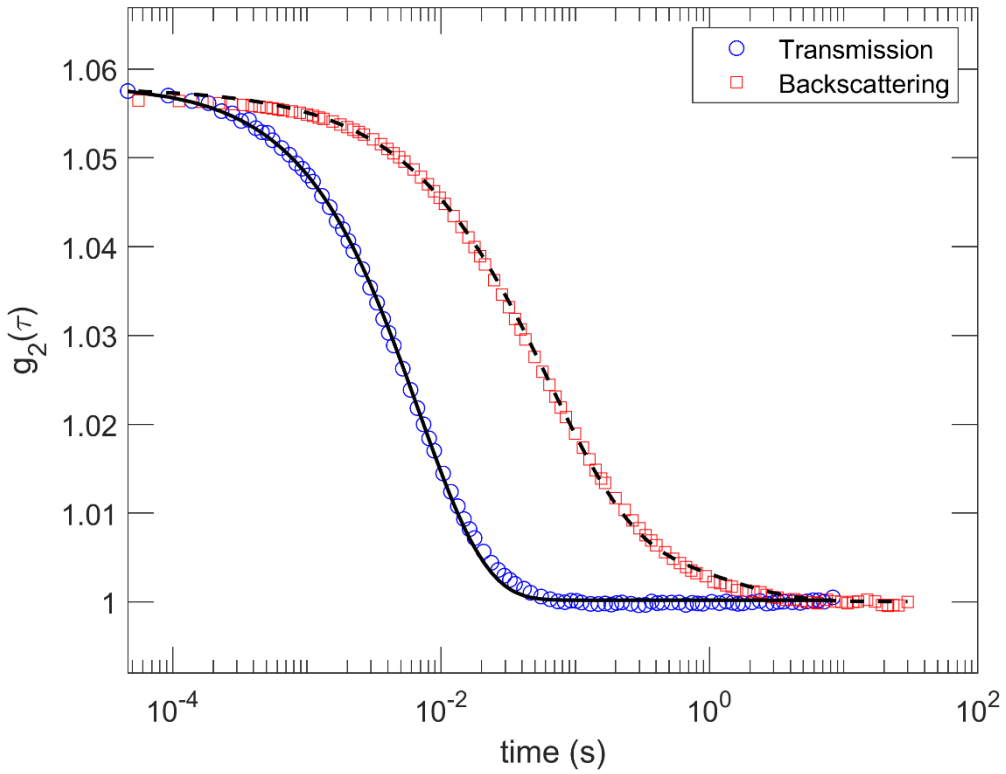

Figure 8 DWS correlation functions in Transmission (blue circles) and Backscattering (red squares) together with the corresponding best fits (black lines) according to Equations 13 and 14. Data acquired from an emulsion of dodecane ($f_{oil} = 0.5$) and water with SDS concentration of $5 \cdot 10^{-3} M$ at $41\ days$ of aging, with DWS Laboratory apparatus described in Section 2.4.3. According to [31] *is imposed* $\gamma = 2.1$ *for this experiment conditions* [47].

MEAN SQUARE DISPLACEMENT AND MECHANICAL PROPERTIES

DWS analysis of correlation function decay allows to obtain a measurement of the mean square displacement that is related to the mechanical shear visco-elastic moduli.

Mean square displacement of scattering centres $\langle \Delta r^2(\tau) \rangle$ is determined by analytical or numerical inversion of generalized forms of $g_1(\tau)$ in Backscattering and Transmission geometry respectively

$$g_{1\,B}(\tau) = e^{-k_0 \gamma \sqrt{\langle \Delta r^2(\tau) \rangle}} \tag{16}$$

$$g_{1\,T}(\tau) = \frac{\frac{L}{l^*} k_0 \sqrt{\langle \Delta r^2(\tau) \rangle}}{\sinh\left(\frac{L}{l^*} k_0 \sqrt{\langle \Delta r^2(\tau) \rangle}\right)} \quad . \tag{17}$$

Both procedures have the pitfall in the determination of baseline and contrast (i.e. plateau and amplitude of the decay of $g_2(\tau)$) to obtain $g_1(\tau)$ from $g_2(\tau)$. Measurements on a time window sufficiently large are required to include dynamics at short and long times. Furthermore, in Equation 16 care must be taken in the determination of γ by considering photons travelled along short paths in the long time because along these paths the central limit theorem used to retrieve $g_{1\,B}(\tau)$ could not hold. In Equation 17 a good knowledge of l^* can be obtained by comparing simultaneous Backscattering and Transmission measurements.

By DWS, one can access to the mechanical shear modulus associated to the mean square displacement of the scattering centres. In a viscoelastic medium, this can be represented as a time dependent quantity $G^*(\tau)$. The real and imaginary part of G^* are the storage modulus G' and the loss modulus G'' respectively describing elastic and viscous response. G^* is related to $\langle \Delta r^2(\tau) \rangle$ by the of Generalized Stokes-Einstein relations which are often written in the Laplace frequency domain [33], [34]

$$G^*(s) = \frac{k_B T}{\pi a \, s \, \langle \Delta r^2(s) \rangle} \tag{18}$$

where s is the Laplace frequency, $\langle \Delta r^2(s) \rangle$ and $G^*(s)$ are the Laplace transforms of $\langle \Delta r^2(\tau) \rangle$ and $G^*(\tau)$, a is the size of the scattering centre, $k_B T$ is the thermal energy.

Then the frequency dependent complex viscoelastic modulus $G^*(\omega)$ is calculated by the analytical continuation obtained by identifying $s = i\omega$, where ω is the Fourier angular frequency and i is the imaginary unit.

There are some difficulties associated with the application of Equation 18 to real data, acquired over a finite temporal window and with limited spatial accuracy. One useful approach, which has been followed in the present study, is to compute the local power law of $\langle \Delta r^2(\omega) \rangle$ as a function of ω on a double logarithmic scale. This is indicated as $\alpha(\omega)$. Then, it has been shown [33] that $G^*(\omega)$ can be calculated as

$$G^*(\omega) \simeq \frac{k_B T}{\pi a \; \langle \Delta r^2(\omega) \rangle \, \Gamma\big(1 + \alpha(\omega)\big) \, i^{-\alpha(\omega)}} \tag{19}$$

where Γ is the gamma-function. Of course, the system is mainly viscous when G'' dominates ($\alpha > 0.5$), on the contrary it is mainly elastic when G'dominates ($\alpha < 0.5$). The limiting cases correspond to $\alpha = 1$ for Newtonian fluid and $\alpha = 0$ for the purely elastic response obeying Hookes'law.

2.4.2 ACCURACY OF DATA ANALYSIS

The accuracy of physical parameters estimated from DWS data is based on the evaluation of the statistical errors on correlation function $g_2(\tau)$. In this research, an estimator of the variance of $g_2(\tau)$ is calculated following the approach described in [35].

Light detection can be accomplished by two classes of detectors: point and multipixel detectors. Average of Equation 7 is performed on time of the speckle fluctuations or over different speckles, respectively. Single point detectors access short time acquisition and uncertainty grows as τ approaches the total measurement time. Strategies to reduce the errors in the correlation function consist on increase the measurement time or the number of photons detected. Multispeckle approach allows the simultaneous detection of several speckles but the time of acquisition is limited by the exposure time. Multipixel detectors in multispeckle scheme decrease the variance by a factor equal to the number of pixels N_{pixels} (ideal condition $N_{speckels} = N_{pixels}$) in case of the camera speed and the incident intensity are sufficient to access the whole temporal window of the correlation function decay. Regarding the calculation of $g_1(\tau)$ via the Siegert relation (Equation 8), both long time baseline and contrast β of the acquired $g_2(\tau)$ need to be determined with accuracy. The baseline at long times requires measurement time much longer than any time scale characteristic of the sample. The value is intrinsically equal to 1 with point detectors which see only one speckle. On the contrary, in the multispeckle acquisition, this does not necessarily happen. The baseline can diverge from unity because of a systematic error introduced when the sample is not uniformly illuminated; the same can also happen for good physical reasons in case of nonergodic samples or when some dynamic is present in the sample which is slower than the accessed experimental time window. The contrast β is defined by the experimental setup. The ideal is to have speckle size comparable to detector size: if the speckle size is larger affects the signal to noise ratio, if it is smaller the contrast decreases due to averaging effects. Point detectors have control on the sensitive area size but for an accurate determination of the contrast is required a long measurement time. For multipixel detectors the fixed pixel size is matched to speckle size that are expanded or reduced using appropriate optics. In the present work, the accuracy of the results analysis has been identified by time and frequency ranges. The limits are imposed on the time window of the field autocorrelation function: the relative error is within 50% when $g_1(\tau)$ remains close to its value at zero and long time.

2.4.3 DIFFERENT DWS SETUPS USED

This Section reports the descriptions of DWS experimental arrangement assembled in the Laboratory of Molecular Nanotechnologies at University of Parma, and of the one implemented on ESA "Soft Matter Dynamics" facility. The SMD instrument was designed for the study of foams, emulsions and granular matter in weightlessness environment, where it is possible to exploit segregation phenomena. This platform integrates an optical microscope, and a Diffusing Wave Spectroscopy apparatus. This DWS apparatus supports single-speckle and multi-speckle acquisition, and also time resolved correlations, to investigate primarily dynamics inside and on the surface of opaque materials. We characterized the performance of the SMD laboratory counterpart [36] available at Airbus, Friedrichshafen, whose features are analogue to the "Flying Model" of the SMD onboard the Columbus module of the International Space Station.

LABORATORY APPARATUS

Figure 9 shows a sketch of the laboratory apparatus. A He-Ne laser (LGK 7665, LASOS Lasertechnik GmbH) with $\lambda = 632.8nm$ and illumination power of 50 mW is used as light source; a linear polarizer and a beam expander are used to polarize the light and enlarge the beam to an area $> 500\ mm^2$ ensuring uniform illumination on the sample. Linear analyzer in Backscattering extinguishes reflected light. Emulsions are observed in a standard quartz cuvette, $1cmx1cm$ of width and thickness respectively, placed on a 3D-printed support made of black polylactic acid that hide cuvette lateral walls from direct illumination. For the emulsions under study, complete randomization of light phase is ensured by cuvette size that is one order of magnitude bigger than l^*. There is no absorption from the sample nor from its container at this light wavelength. Samples are stored in a temperature controlled chamber $(20 \pm 0.1°C)$ and placed on a temperature-controlled holder during the experiments. Light in Backscattering and Transmission geometry is collected by two CMOS linecameras (Basler Racer raL2048-48gm, Basler AG with pixel size 7 μm, 2048 $pixels$, minimum lag time 12.4 µs, 12 bit digitizer) equipped with objective lenses that focus on the cuvette walls by varying focus and iris. Laser stability is ensured by turned on the laser and start the acquisition after 30 min; other external fluctuations are prevented by fixing all components onto a pneumatic antivibration optical table (CINEL srl).

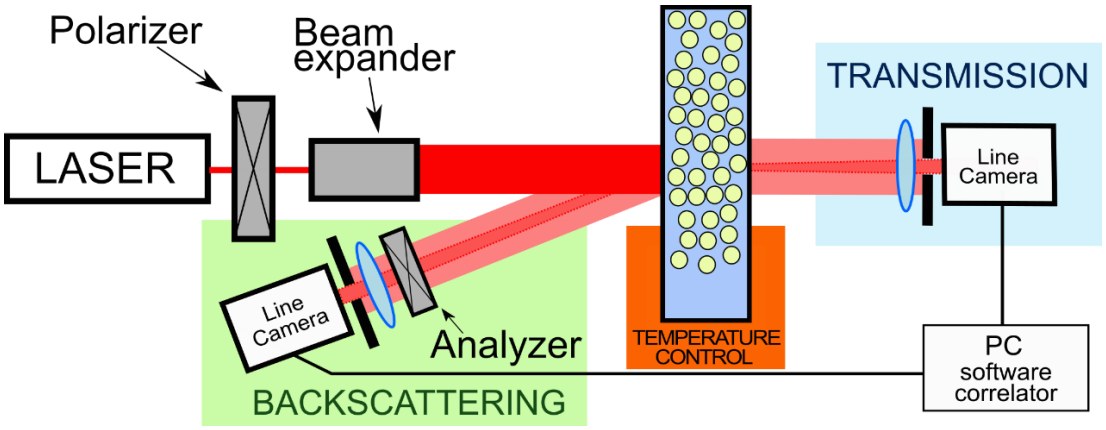

Figure 9 Sketch of the DWS setup used for laboratory experiments. Backscattering and Transmission measurements were performed simultaneously by recording images using two linecameras. Cameras are equipped with an objective with adjustable focal lens and diaphragm, and a linear analyzer in Backscattering to extinguish reflected light. Images are processed through a PC running a multi-tau software correlator. Figure adapted from [35].

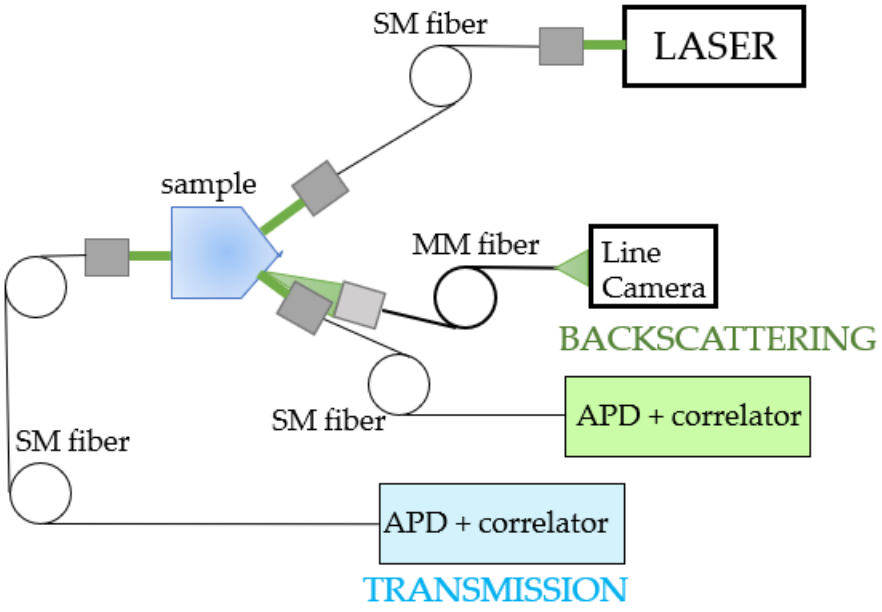

Figure 10 Sketch of the DWS setup implemented on Soft Matter Dynamics facility. Light from a leaser reaches the sample via a single mode (SM) optical fiber. Two APD modules with correlator detect Backscattering and Transmission signals by conveying light through monomode optical fibers; a linecamera collects light conveyed by a multimode (MM) optical fiber in Backscattering.

"SOFT MATTER DYNAMICS" ONBOARD THE ISS AND ITS LABORATORY COUNTERPART

The "Soft Matter Dynamics" facility is upload onboard the ISS in the Fluid Science Laboratory of the Columbus modulus. On-ground experiments have been performed at AIRBUS Defence and Space in Friedrichshafen [36] using a SMD reproduction developed to test the SMD functionality (Figure 11).

In this apparatus, shown in Figure 10, the light source is a linear polarized Nd:Yag laser (*Cobolt AB*) with $\lambda = 532nm$ and illumination power of $300\,mW$. Through a single mode optical fiber light impinges the sample over an area of $1.5x1.5\ mm^2$ *a*long the first direction of the sample cell. Light detection is ensured by two avalanche photodiode modules (APD) coupled in Backscattering and Transmission; and one CMOS linecamera (Basler Runner ruL1024-19gm with pixel size $10\,\mu m$, $1024\,pixel$, minimum lag time $50\,\mu s$, $12\,bit$ digitizer) in Backscattering. Each APD module integrates four independent APDs and is coupled to a digital correlation board (ALV CorrTector, ALV GmbH) for signal auto-correlations and cross-correlations. Light is conveyed by multimode fiber to the linecamera and by monomode optical fibers to the APD modules, matching speckle size and pixel size. Figure 12 shows the sample cell, it is made of polycarbonate and has a volume of $11mm \times 14mm \times 11mm$. The Figure shows the magnetic piston for emulsification process within the sample cell, and the metal case accommodating four of these units when they are inserted in the facility. The metal case has two windows for light illumination and detection; it is hosted onto a carousel tray (maximum 5), which moves the desired sample cell in measurement position. Temperature control of the facility is within $1°C$.

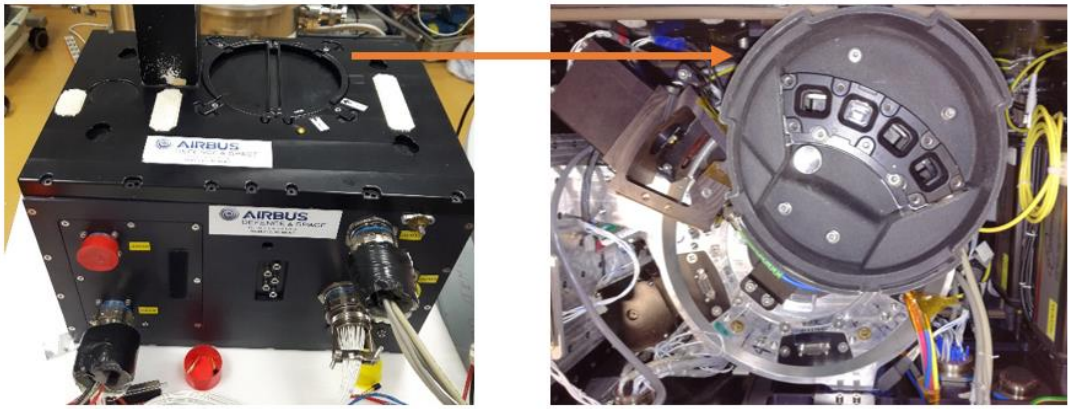

Figure 11 Front and top overview of the SMD laboratory counterpart at AIRBUS Defence and Space in Friedrichshafen.

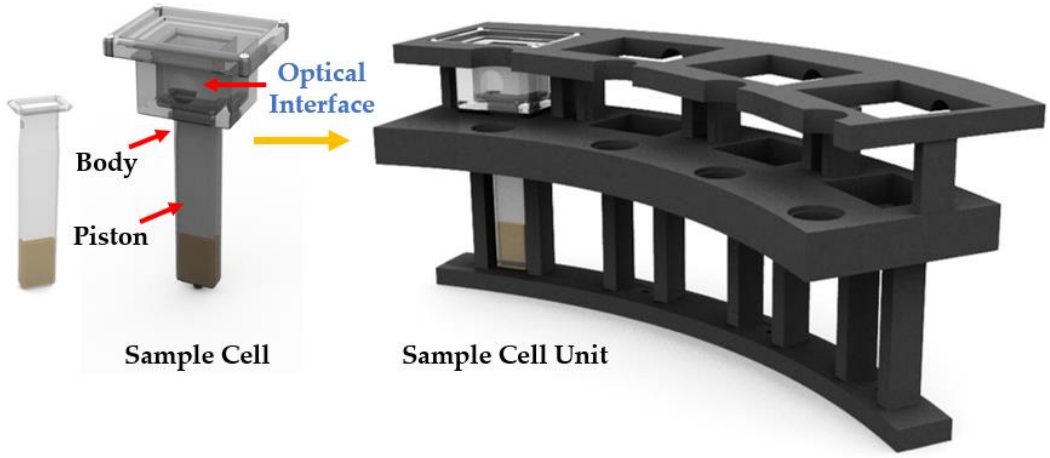

Figure 12 From left to right sketch of: piston, sample cell body, and the sample cell unit where it is enclosed.

3. CHEMICALS USED

In this research, the solutions are always made with high purity water produced by a Millipore (Elix + MilliQ) purification chain providing surface tension =72.5mN/m at 20°C and stable over long time. For model emulsions, dodecane is used as the oil phase. It is an alkane hydrocarbon with low volatility. It was purchased from *Sigma-Aldrich* with highest purity degree and utilised without further purification. For food-grade emulsions, we used a medium chain trigliceride (MCT) oil obtained from an industrial company (Eulip, Parma, Italy) and purified from the presence of impurites or surface-active contaminants by filtrating twice by an activated aluminia column. For all components, purity was checked by long time measurement of dynamic interfacial tension. Stable values of 53 mN/m and 19.3 $\mp$ 0.2mN/m at 20°C were found for water/dodecane and water/MCT interfaces, respectively.

As explained in Section 1.2, the polarity and the type of the surfactant head group (ionic or non-ionic surfactants) and its concentration both influence emulsion stability because the surfactant surrounds dispersed droplets providing a sort of barrier that prevents their aggregation. The chemical structures and properties of the surfactants used in the experiments are listed in Table 1. The concentration of surfactants in the solution is expressed using the square-bracket notation [ ].

All surfactants were used without further purification.The anionic surfactant, SDS, has been investigated at water/dodecane interface as well as stabilizer for dodecane-in-water emulsions [9]. With time, SDS produces dodecanol by hydrolysis: a high surface-active molecule which may co-adsorb with SDS [37]. Using dodecane however ensures dodecanol transfer in the oil phase without affecting the adsorption. The interaction between aliphatic chains of the oil and surfactant is a driving forces determining the behaviour of interfaces. For food-grade emulsion, synthetic surfactants of sorbitan esters, such as Tween80, are used within MCT oil [38], [39].

Table 1 Chemical formula and properties of the surfactants used for the experiments.

<table>
<tr><th colspan="2">IONIC SURFACTANT</th></tr>
<tr><td colspan="2">Sodium dodecyl sulfate
SDS
Sigma-Aldrich</td></tr>
<tr><td colspan="2">$CMC = 8.2\ mM$
 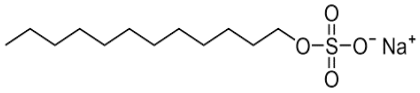 </td></tr>
<tr><th colspan="2">NON-IONIC SURFACTANTS</th></tr>
<tr><td>Polyoxyethylene (5) decyl ether
$C_{10}E_5$
(Nikko)</td><td>n-dodecyl-β-D-maltoside
$\beta - C_{12}G_2$
(Fluka)</td></tr>
<tr><td>$CMC = 0.84\ mM$ ($k_P(\frac{water}{hexane})$ = 13,9)[40]
  </td><td>$CMC = 0.22\ mM$
 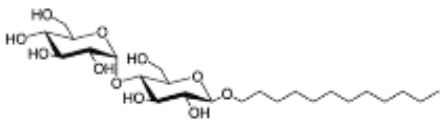 </td></tr>
<tr><td>2-propylheptyl octaethylene glycol eter
Ethylan1008
(AkzoNobel)</td><td>Polyoexythylene sorbitan esters
Tween80
(Sigma-Aldrich)</td></tr>
<tr><td>$CMC = 2\frac{g}{l}$, biodegradable
 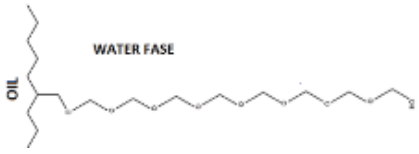 </td><td>$CMC = 0.012\ mM$
 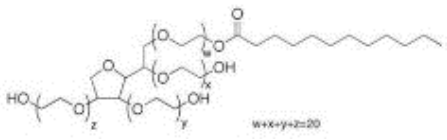 </td></tr>
</table>

4. THE EMULSIFICATION PROCESS

Emulsification is usually achieved by the application of mechanical energy, necessary to increase the interfacial area between the two liquids. Mechanical energy causes droplets to break-up, leading to generation of new smaller droplets. This new interfacial area must be covered by the surfactant molecules present in the bulk in order to stabilise the obtained emulsion. Given the ingredients, the emulsification technique results in emulsions with different properties. The emulsification process has two critical parameters that differentiate emulsions: the specifications of the mechanical stress applied, and the emulsion components.

To study the effects on the structure and aging of the emulsion, different campaigns of different emulsification methods (described individually in Sections 4.1.1,4.1.2,4.1.4,4.1.5) have been conducted. Droplets size distribution and stability in time have been investigated by emulsifying through:

- rotor-stator homogenizer at University of Parma;
- syringe forcing at University of Parma;
- pulsating emulsification device reproduction of SMD facility onboard the ISS tested at AIRBUS Defence and Space in Friedrichshafen;
- pulsating emulsification device manufactured and tested in the Laboratory of Chemical Technology at Aristotle University of Thessaloniki (AUTH).

Emulsion stability was monitored through macro imaging and digital image elaboration, while optical microscopy was used for statistical analysis of droplets size. Results were used to validate the DWS technique.

In Section 4.2 emulsification techniques and chemical ingredients effectiveness are discussed. For each technique several experiments have been conducted varying the energy and time of emulsification, the surfactant quantity and the oil volume fraction f_{oil}, while the temperature was kept constant at $\sim 20°C$.

4.1.1 ROTOR-STATOR HOMOGENIZER

The rotor-stator homogenizer is composed by a metal rotor, which rotates inside a metal casing (stator). It is immersed into the liquids within a cylindrical tank. This high-energy emulsification technique generates emulsion with droplet size of the order of microns. The rotation of the rotor draws liquid into the space between the rotor and stator where they are subject to high shear forces, due to change in velocity in this space, that are driving forces for droplets disruption. Mixing conditions are controlled by varying the rotation speed and duration. There is not a maximum volume which can be processed but for best results a moderate volume ensures a uniformly and completely homogenization. By increasing rotational speed and decreasing diameter of the container the interfacial area increases [5]. Emulsification might incorporate gas bubbles, leading to the formation of drop-bubble aggregates that make the system more stable.

As rotor-stator homogenizer we used an Ultraturrax mixer (IKA ULTRA TERPAX T25). It provides rotation speeds up to 10000 rpm. The volume of the mixture in glass beakers is 20 ml and the mixing time is 10 min (Figure 13). It is cleaned after each use with ethanol and high purity water.

Figure 13 The Ultraturrax homogenizer used for emulsification.

4.1.2 SYRINGE SYSTEM

A syringe is filled with oil phase; the syringe needle of diameter 2 mm is immersed in a cylindrical tank containing the aqueous phase with surfactant dispersed (Figure 14). The emulsion is created by pumping for 10 times the fluids through the syringe creating the shear force needed for droplet breakage. Care is taken in keeping the needle always immersed in the aqueous phase, and by regulating the speed of sucking and emptying in order to minimize the presence of air bubble in the emulsion. Being user-dependent, the technique is affected by weak reproducibility and the pressure inducing shear force is very low, leading to the formation of large droplets (typical size in the range $10 - 20\ \mu m$).

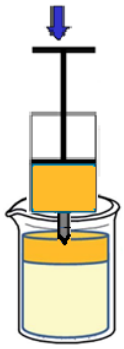

Figure 14 Sketch of the syringe emulsification system.

4.1.3 DOUBLE SYRINGE SYSTEM

The aqueous and oil phases were loaded separately in two syringes, that have been connected and the emulsification results by alternately pushing (10 $times$) the syringe pistons (Figure 15). The shear force leads to droplet formation. This technique avoids the presence of air but remains weakly controlled as the previous one.

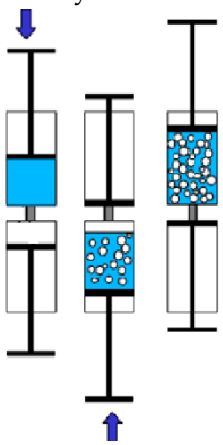

Figure 15 Sketch of the double syringe emulsification system.

4.1.4 PULSATING PISTON: SMD LABORATORY COUNTERPART

A pulsating emulsification device reproduction of SMD has been developed as verification test facility [36] to demonstrate its functionality. It is analogous to the SMD described in Section 2.4.3 with an opening cap to access and insert the sample cell unit in the right position by hand. Figure 16 shows photos of the device at AIRBUS Defence and Space in Friedrichshafen.

The sample cell body is filled of the aqueous phase first and the oil phase later from the top (total volume 3 ml). The piston is inserted avoiding liquids leakage and the cell is closed by a top cover (Figure 11). Once the sample cell is placed in the sample cell unit within the experimental container of the facility, piston shaking is activated. The piston contains a permanent magnet. It is moved up and down by an external magnetic field generated by two coils. The emulsion is generated by the shear forces created in the gap (0.6 mm) between sample cell wall and the plate of the piston. The maximum frequency of the piston speed is 10 Hz.

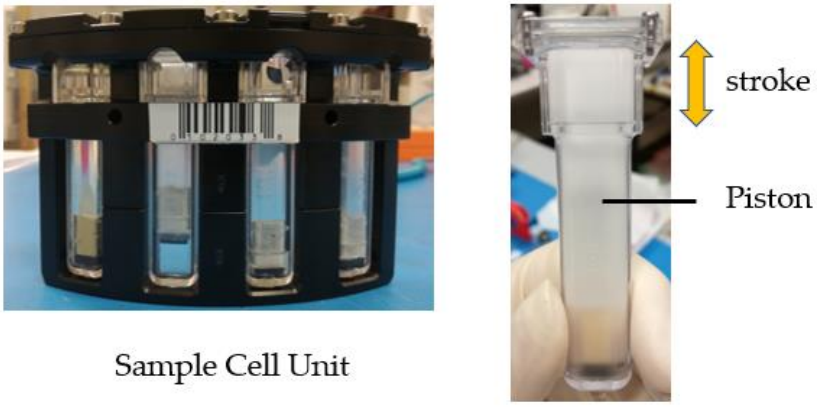

Figure 16 Pulsating piston device used for microgravity experiments. a) The SMD laboratory counterpart at AIRBUS Defence and Space in Friedrichshafen, b) the sample cell unit and c) the sample cell with piston included for pulsation.

4.1.5 PULSATING PISTON: AUTH EMULSIFICATION DEVICE

This emulsification device is a laboratory counterpart of SMD manufactured in the Laboratory of Chemical Technology at Aristotle University of Thessaloniki (AUTH). It has been developed for reproducing the same emulsification features of the SMD facility: a piston pulsation producing shear forces along the narrow gap between piston plate and side walls. The cell has dimensions similar to SMD sample cell, it is rectangular with its main body made in aluminium whereas the cell walls are made of glass. Its cross-section is scavenged by a thin aluminium plate fixed at the tip of a piston that moves up and down in the cell at controlled frequency (maximum 15 Hz) and duration. The gap between plate and walls is 0.2 mm.

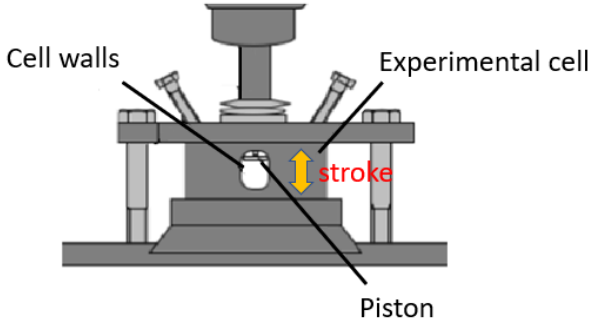

Figure 17 Sketch of the pulsating emulsification device implemented in Laboratory of Chemical Technology at Aristotle University of Thessaloniki (AUTH).

4.2 EFFECTIVENESS OF THE EMULSIFICATION PROCESSES

EFFECTS OF TECHNIQUE AND EMULSIFICATION TIME

Figure 18 shows the temporal evolutions of emulsions composed by dodecane and water ($f_{oil} = 0.5$) stabilised with $[SDS] = 2\ mM$, produced by varying emulsification technique: syringe, aqueous and oil phases separate within $2\ hours$. This is not observed for emulsions obtained with greater shear forces: they reach the same final emulsion volume fraction (70%) in $2\ hours$ and remain stable for several days. A tendency to separate faster is observed for samples emulsified with the pulsating device, when emulsification time is decreased from $10\ min$ *to* $2\ min$ and $30\ s$. Droplets size distributions, see Figure , confirm that increasing agitation energy or duration of emulsification give more control over the droplet dispersity.

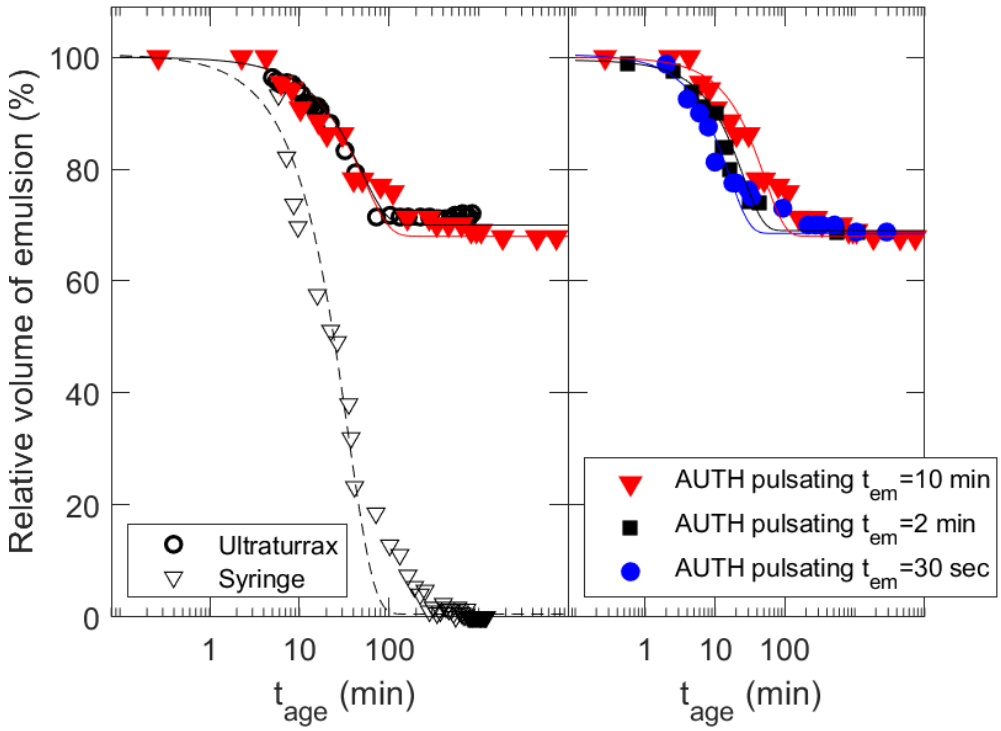

Figure 18 Temporal evolution of the emulsion fraction: left) emulsification with Ultraturrax homogenizer at $10000\ rpm$ *for* $10\ min$*, syringe and AUTH pulsating device at* $f = 10\ Hz$*; right) AUTH pulsating device for a duration of* $30\ s, 2\ min, 10\ min$*. Emulsions are dodecane in water with* $f_{oil} = 0.5$ *and* $[SDS] = 2\ mM$*. Data from macro imaging analysis (symbols) are fitted with a trend line (*$f = baseline + contrast \cdot erfc(t/\tau)$*).*

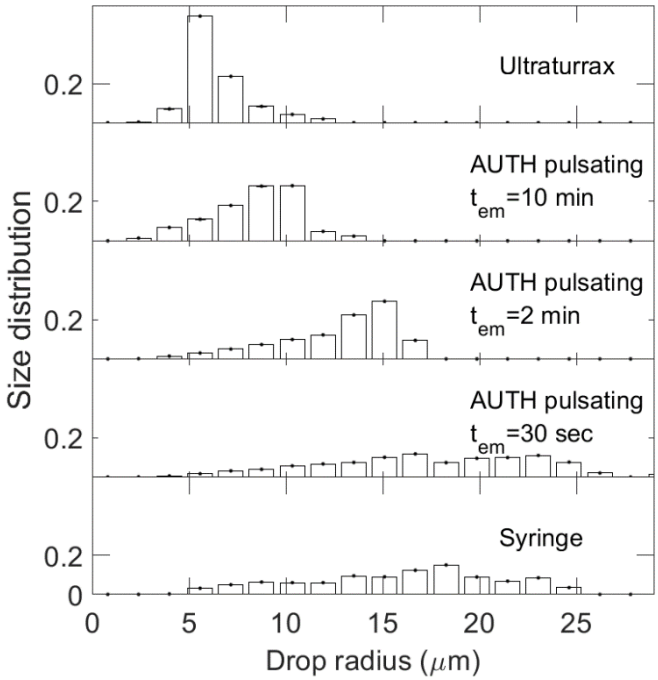

Figure 19 Histograms of the drop radius distribution weighted by volume as measured by micro imaging for the same data of Figure 18.

Furthermore it was verified, see Figure 19, that a two step pulsation, 5 s at 2 Hz followed by10 min at 10 Hz, yields a monodispersed drop size distribution, but also a faster oil separation. This might be due to the creation in the first step of bigger drops that are subject to coalescence and creaming before the start of the faster emulsification step.

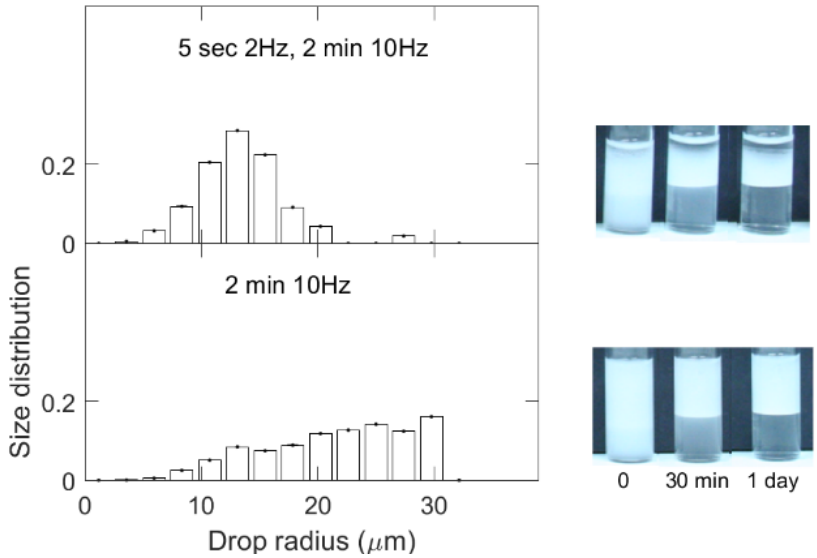

Figure 20 Histograms of the droplet size distribution weighted by volume and aging of emulsions with $f_{oil} = 0.5$ *and* $[\beta - C_{12}G_2] = 0.11\ mM$ *obtained with AUTH pulsating device following two procedure: top) two step pulsation,* 5 s *slow* ($f = 2\ Hz$) *before 10 min fast* ($f = 10\ Hz$)*; bottom) one step pulsation of* 2 min *at* $f = 10\ Hz$

EFFECTS OF CHEMICAL COMPOSITION

Examples of stable emulsions obtained by mixing dodecane and SDS in water with Ultraturrax are reported below. After an initial time in which emulsions are affected by creaming, the emulsion volume fraction reaches a value that remains constant for more than 1 $week$. Figure 21 shows the emulsion volume fraction increasing from 40% to 90% as the initial oil fraction increases from 0.3 to 0.7, respectively. The dodecane phase in these cases is completely emulsified.

For emulsions with oil fraction $f_{oil} = 0.5$, Figure 22 illustrates the time evolution of the emulsion fraction at different values of SDS concentration, as well as a comparison of the droplet size distribution with images taken by microscopy. For a time of the order of 100 min, a decrease of emulsion height is observed. It reaches a stationary state weakly dependent on the surfactant concentration. A decrease of SDS concentration is associated with broader droplet size distributions, and with an increase in the average size.

Other chemical compounds are investigated with pulsating piston device. The behaviour of Ethylan1008 and SDS is comparable showing a slower aqueous separation and no oil phase separation, while $\beta - C_{12}G_2$ and $C_{10}E_5$ show oil phase separation after days and hours respectively. Indeed the drop size distributions are broader (Figure 23).

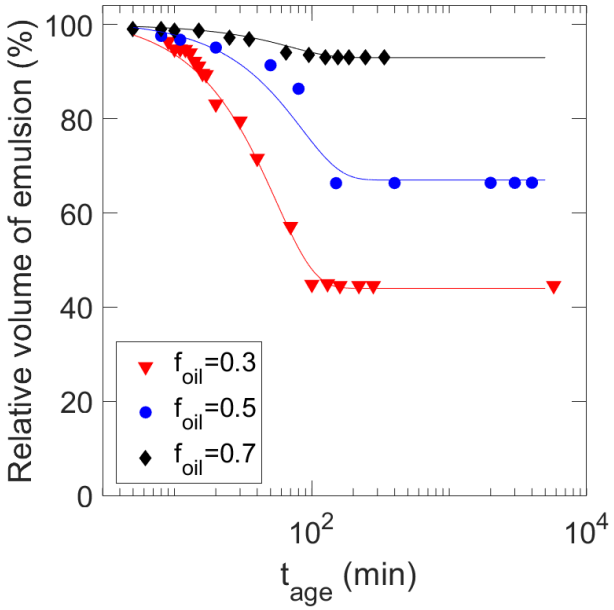

Figure 21 Comparison of time evolution of the emulsion fraction for samples emulsified with Ultraturrax at $f = 10000\ rpm$ *for* $10\ min$ *starting from oil volume fraction of* $0.3, 0.5$ *and* 0.7 *with* $[SDS] = 7 \cdot 10^{-4} M$. *Data from macro imaging analysis (symbols) are fitted with a trend line* ($f = baseline + contrast \cdot erfc(t/\tau)$).

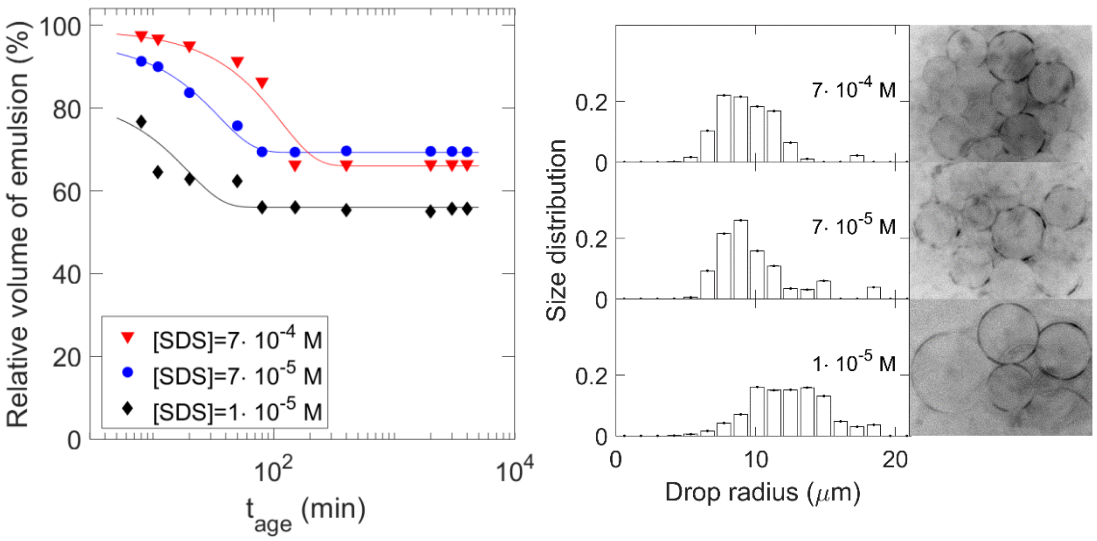

Figure 22 Comparison of emulsions with $f_{oil} = 0.5$ emulsified with Ultraturrax at $f = 10000\ rpm$ for $10\ min$ at different concentration of SDS. Left) Temporal evolution of the emulsion fraction; right) histograms of the drop radius distribution weighted by volume and pictures taken by micro imaging analysis. Data from macro imaging analysis (symbols) are fitted with a trend line ($f = baseline + contrast \cdot erfc(t/\tau)$).

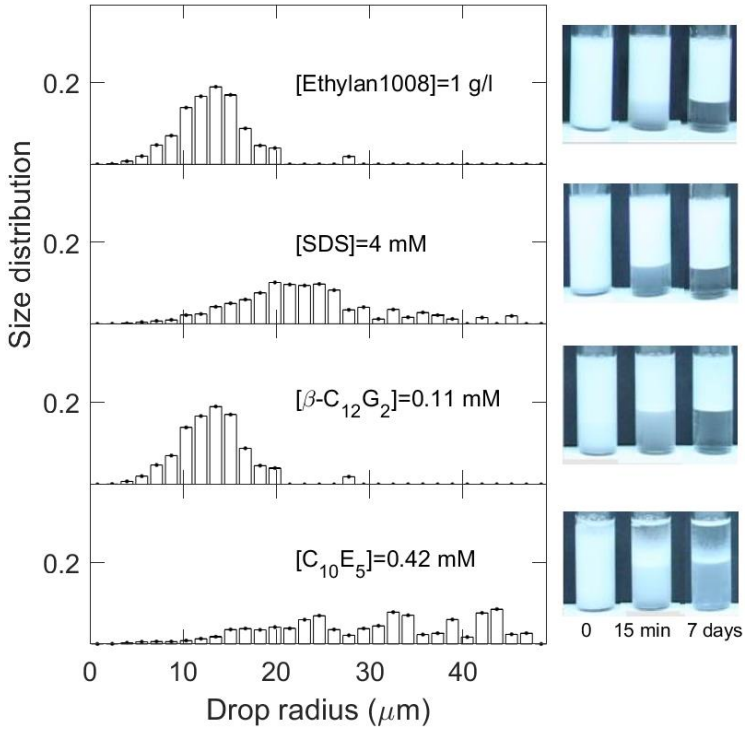

Figure 23 Histograms of the droplet size distribution weighted by volume and aging of dodecane in water emulsions obtained with AUTH pulsating device for 2 min at f=10 Hz for different surfactants dispersed in the water phase at concentration equal to half CMC.

Finally, the stability of an emulsion made of food-grade ingredients emulsified by double syringe method is studied. Results confirm the possibility to develop formulations of food-grade oil-in-water emulsions stable for several days even at low surfactant concentrations using low energy emulsification techniques. Stability and time evolution as a function of Tween80 quantity in emulsions with $f_{oil} = 0.5$ are shown in Figure 24. Oil and water phase separation takes place after few minutes for [Tween80]$< 1 \cdot 10^{-5} M$, while stable emulsions with slow water drainage are obtained for [Tween80]$> 4 \cdot 10^{-5} M$. Further investigation is needed to interpret the emerging features. The equilibrium and the dynamic interfacial tension data have to be modelled taking into account the exchange between the liquid phases of this non-ionic surfactant.

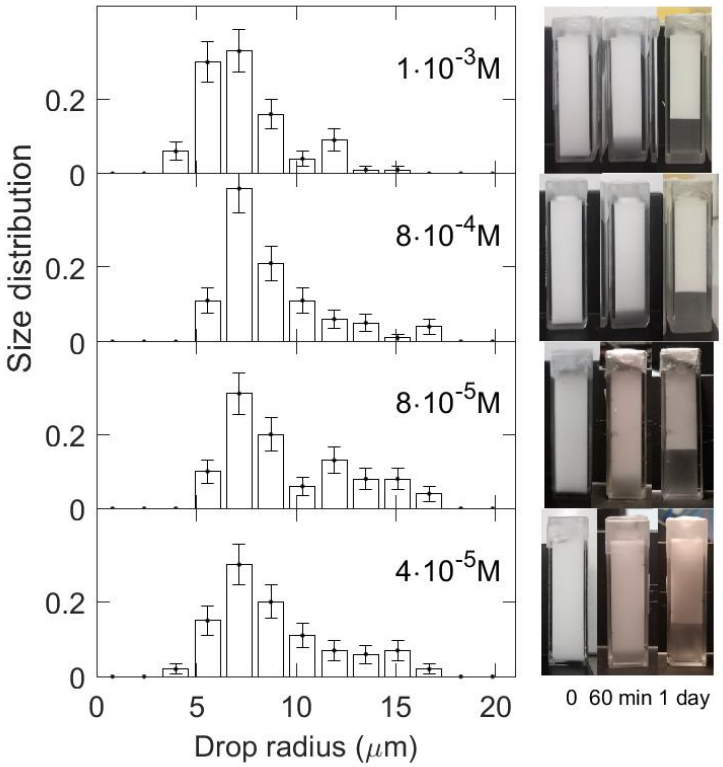

Figure 24 Histograms of the droplet size distribution and aging of MCT in water emulsions ($f_{oil} = 0.5$) obtained with double syringe method varying [Tween80] from $4 \cdot 10^{-5}$ to $1 \cdot 10^{-3}$ M.

5. CHARACTERIZATION OF A PARADIGMATIC OIL-IN-WATER EMUSION

This Section reports on the long-term stability of a paradigmatic oil-in-water emulsion with low surfactant content, characterized to explain the mechanisms involved in emulsion formation and stability in terms of droplet processes at the interface. A multiscale investigation of internal dynamics and structure gives insight on the intimate link between microscopic properties of surfactant layers and macroscopic properties of emulsion. In Section 5.2, adsorption properties at the droplet interface are reported. In Sections 5.3 and 5.4, aging and mechanical properties of the respective emulsions have been investigated by micro imaging, macroscopic image of the thickness of the emulsion layer, and DWS. Results are discussed in Section 5.5.

5.1 EMULSION COMPOSITION AND PREPARATION

Emulsions have been produced by mixing dodecane ($f_{oil} = 0.5$) and water with SDS through Ultraturrax (Section 4.1.1) at $10000\ rpm$ for $10\ min$. SDS concentration was varied between $2 \cdot 10^{-5}$ and $5 \cdot 10^{-3} M$,i.e. below the critical micellar concentration ($CMC = 8.2 \cdot 10^{-3} M$). The emulsions are produced in $20\ mL$ glass beakers using a total amount of liquid of $20\ mL$. After emulsification, sample portions are immediately transferred in quartz cuvettes for DWS, micro and macro imaging characterizations.

5.2 ADSORBED LAYER DYNAMICS

Adsorption properties of SDS at water-dodecane interface are characterized by interfacial tension and dilational rheology measurements using the technique described in Section 2.1.2. These results are utilized in [9] to interpret the behaviour of interacting droplets related to coalescence or to the evolution of drop size related to Ostwald ripening, in order to understand the relation with the relative emulsions stability.

The equilibrium interfacial tension at the water-dodecane interface is reported in Figure 25. The CMC value obtained is $8.2 \cdot 10^{-3} M$. The best-fit used to interpret the

equilibrium surface tension of SDS is the two-state adsorption model [41], [42]. This theoretical adsorption isotherm assumes a reorientation of SDS resulting from the interaction between alkyl tails and/or with the oil molecules [43]. The presence of "gauche defects" in the alkyl chain [43] allows SDS molecules to bend. Thus, at small coverage (low surfactant concentration in the solution) they adsorb occupying a larger area (for sake of simplification one can model that they lie parallel to the interface), by increasing the coverage, they preferably adsorb occupying a smaller area, orienting vertically under the effect of the packing. Surface pressure ($\Pi = \gamma_0 - \gamma$) and the total adsorption Γ are related through the equilibrium equation

$$\Pi = -\frac{RT}{\omega}\ln(1 - \Gamma\omega) \tag{20}$$

where $\omega = (\omega_1\Gamma_1 + \omega_1\Gamma_2)/(\Gamma_1 + \Gamma_2)$ is the average surface molar area weighted by the two different areas per mole ω_1 and ω_2. The equilibrium of the system is also described by the relation with the surfactant concentration c

$$bc = \frac{1 - e^{-\Pi w/RT}}{\left(\frac{\omega_1}{\omega_2}\right)^{\alpha} e^{-\frac{\Pi\omega_1}{RT}} + e^{-\frac{\Pi\omega_2}{RT}}} \tag{21}$$

where the parameters b and α depict the surface activity of the two state.

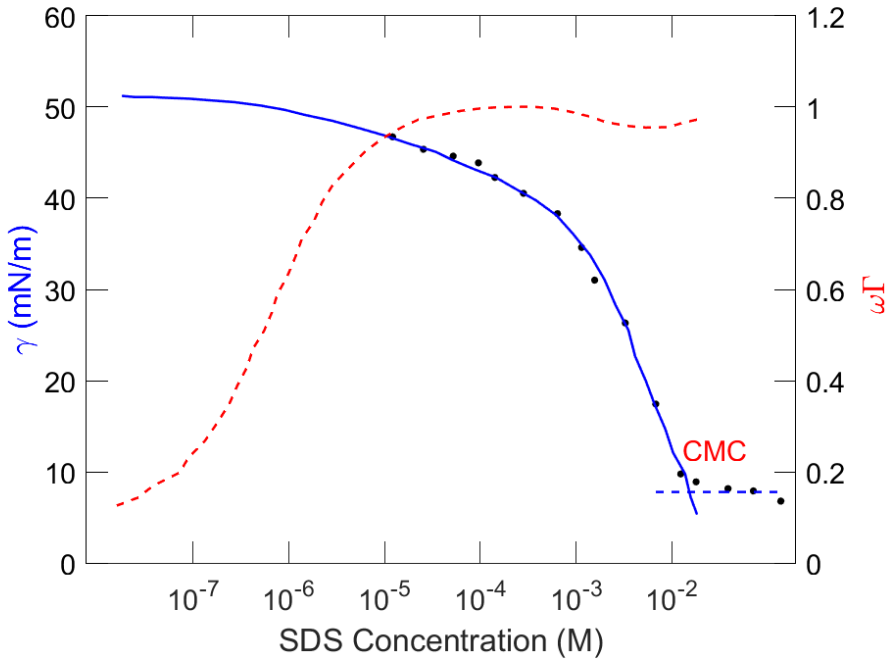

Figure 25 SDS dependence of equilibrium interfacial tension (black point, left y-axis). Best-fit isotherm from the two state model (blue curve, left y-axis) and relative surface coverage (dashed red curve, right y-axis).

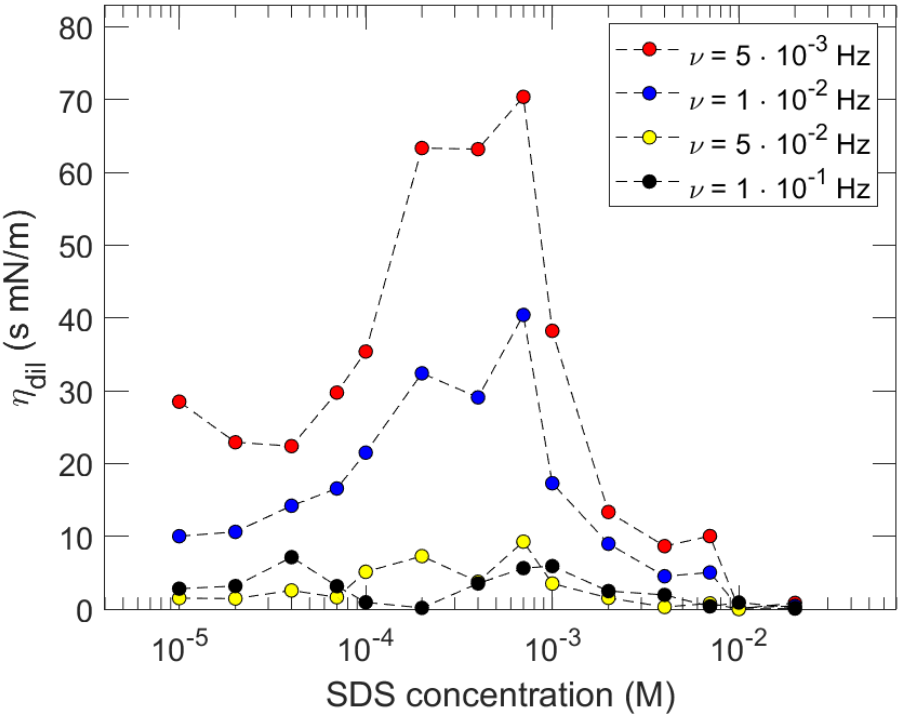

Figure 26 SDS dependence of the dilational viscosity for different values of frequency. The estimation of the error on the measurements is discussed in the text.

Surface coverage is calculated from the isotherm parameters of the fit: surfactants cover all the surface (red curve) $\omega\Gamma = \omega_1\Gamma_1 + \omega_1\Gamma_2$ at concentration well below the CMC.

In [9] dilational viscoelasticity is calculated from Equation 6 for frequency ν spanning in the range $5 \cdot 10^{-3} - 0.1\ Hz$. From the imaginary part of the dilational modulus, dilational viscosity is given by

$$\eta_{dil} = \frac{E_i}{2\pi\nu} \ . \tag{22}$$

It reflects the rheological response of the adsorbed layer; it is governed by diffusion of the surfactant between the interface and the bulk that re-equilibrate the concentration profile and interfacial relaxation caused by molecular reorientation. Figure 26 shows the dependence on the SDS concentration at different values of frequency in a range from $5 \cdot 10^{-3} to\ 0.1\ Hz$: the tendency exhibits an increase up to a maximum, followed by a decrease toward zero. Dilational response grows as surfactant concentration increases, i.e. the variation of interfacial tension, following the slope of the isotherm, passes through a maximum and vanishes when it is contrasted by diffusion process at higher concentrations [9]. It is worth to notice that the position of the maximum is quite independent of the frequency. Based on the error

on the measured interfacial tension, estimated in $\pm 0.5\, mN/m$, the error on the reported dilational viscosities is $0.5/(2\pi v)$.

Experiments of drop coalescence have been performed by put in contact and force together two droplets of dodecane immersed in an SDS solution [9]. It was recorded by a camera in an optical microscope designed in the Laboratory ICMATE-CNR in Genova. Droplets have been formed at the tip of small stainless steel capillaries (diameters of $1-2\, mm$) and the growth has been controlled by high-precision syringes. It has been observed coalescence with surfactant concentration of $1 \cdot 10^{-7} M$ after the formation of the drop; whereas for $[SDS] > 1 \cdot 10^{-6} M$ coalescence is avoided also after $100\, s$ and even when the drops are pressed one against the other. Results confirm that SDS hinder coalescence also at concentration well below the CMC. This is explained in terms of electrostatic repulsion due to surfactant layers at the liquid film between droplets, and for the large surface coverage provided by surfactant molecules reorientation.

Experiments of drop size evolution at different degrees of emulsion destabilization have been obtained by Dynamic Light Scattering (DLS) [9]. They are used to study processes involved in the evolution of emulsions. Samples are diluted by a factor of 10 with the corresponding SDS solution and analysed in the transient phase, when the creaming process is no more relevant, and the larger droplets are away from the acquisition zone. It was observed an increasing linear dependence of the estimated average drop radius and time. This corresponds to a linear increase of drop volume related to Ostwald ripening process appreciable only for a population of droplets under micrometric size at long timescale.

5.3 TEMPORAL EVOLUTION OF THE EMULSIONS

Emulsions stability and creaming were investigated on the macro scale by imaging. Time evolution of the emulsion fraction is reported in Figure 27. For emulsions at lower SDS concentration also the water and oil phase separates in the 10 *days* of aging. Emulsion layer results clearly distinguishable from drained water after the first hours, in which the dynamic is mainly dominated by creaming of the oil drop. At this aging it is referred as Regime I).

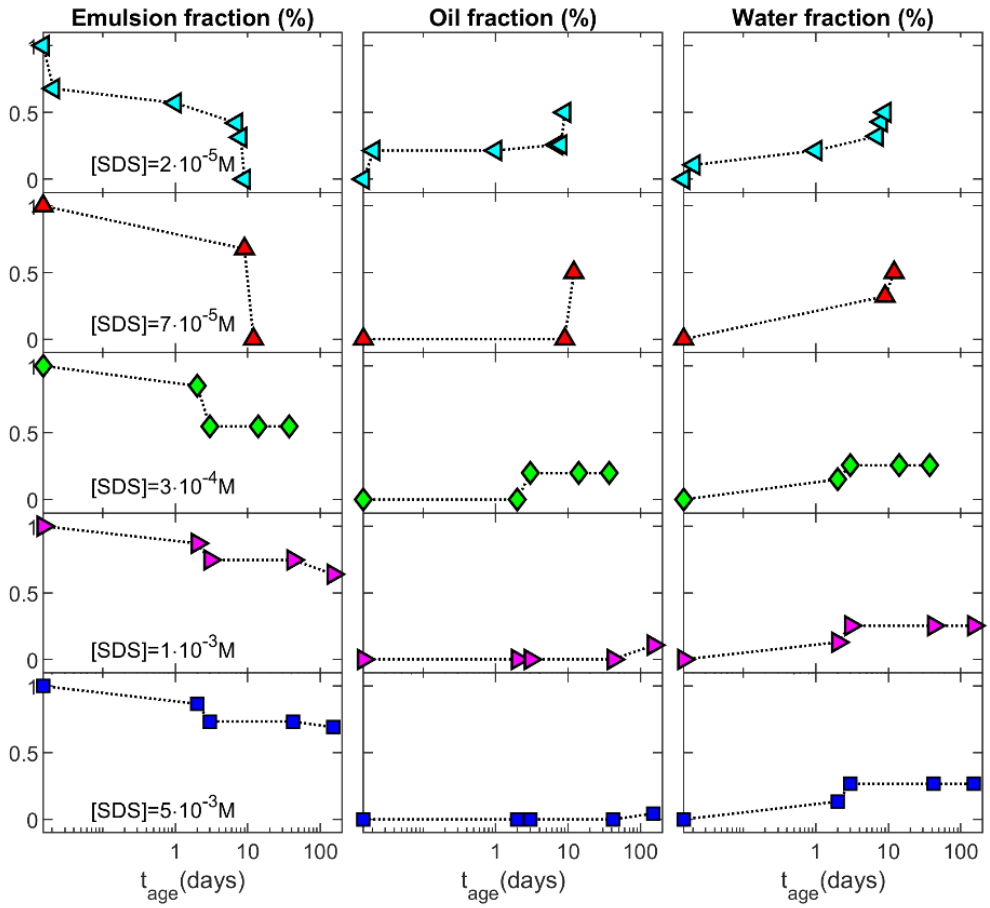

Figure 27 Temporal evolution of the emulsion, oil and water fraction: samples with lowest [SDS] concentration show phase separation in 10 *days.*

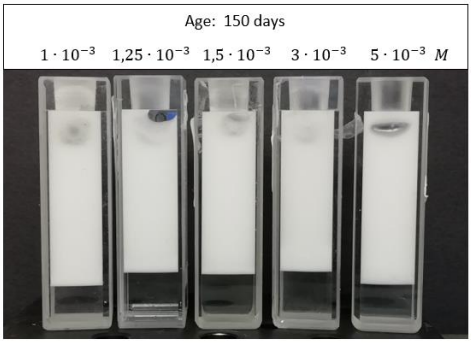

Figure 28 Picture of emulsions with higher [SDS] concentration still stable in Regime III) $\sim 5\ months$. *Figure taken from* [47].

DWS analysis focused on the following regimes and in particular on the laws governing deceleration of the dynamics as aging proceeds:

- Regime II) corresponds to the firsts 10 $days$ of aging when oil creaming and water drainage are completed, and the water layer is completely transparent. There is no macroscopic evolution observed on the macroscopic scale, but deceleration of the dynamic observed by DWS as aging proceed.

- Regime III) can only be observed for more stable emulsions with concentration of $[SDS] > 3 \cdot 10^{-4} M$. Figure shows these emulsions that do not decompose after 150 $days$ of aging. Macro evolution of the morphology is not observed, while the dynamic from DWS continues to slow down following a power-law dependent on time. At this regime a relaxation process slower than 100 s in Backscattering geometry is also observed. In this case the correlation functions have been fitted by introducing the slower decay τ'_B

$$g_{2,B}(t) = 1 + \beta \left(f e^{-2\gamma \sqrt{\frac{6t}{\tau_B}}} + (1-f) e^{-2\gamma \sqrt{\frac{6t}{\tau'_B}}} \right) \tag{23}$$

  with f indicating the fraction of the total contrast ruled by the "main" dynamics decay, while $(1-f)$ is the frozen contrast that was found $< 20-30\%$ in all cases. The origin of this process could be associated to slow relaxation due to rare events, for example coalescence or rearrangements.

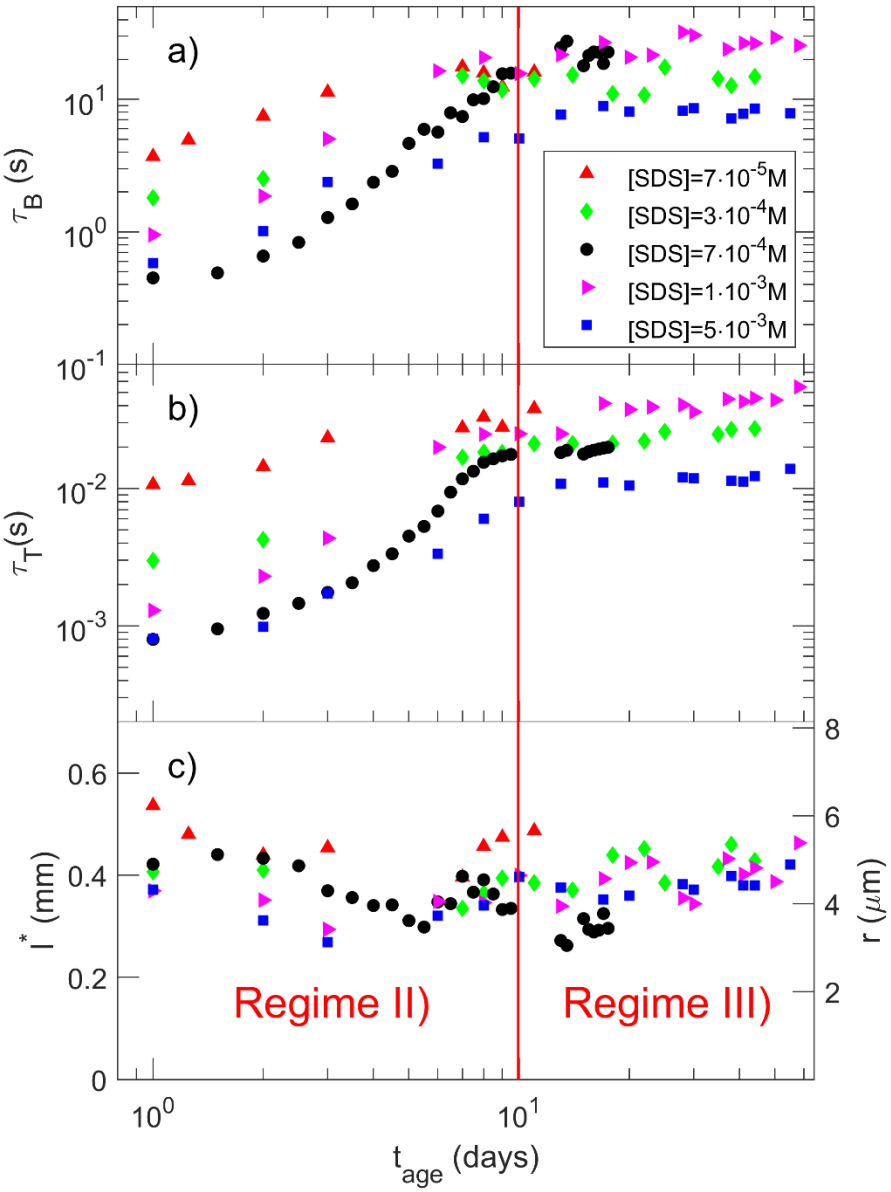

Figure 29 Aging evolution of a) Backscattering relaxation time τ_B, b) Transmission relaxation time τ_T and c) transport mean free path l^*(left y-axis) and deduced average radius of drops r (right y-axis). The parameters were obtained by fitting DWS measurements of emulsions at different SDS concentration. Figure adapted from [47].

Relaxation times τ_B and τ_T, the transport mean free path l^* proportional to their ratio, and the estimated average drop radius r are shown in Figure 29. In Regime II) the increase of both relaxation times by two orders of magnitude indicates a deceleration of the dynamics, that is not explained in terms of structural changes as l^* remains nearly constant. As observed in Section 4.2 the emulsification technique influences the dimension of the droplets produced that not varies with the concentration of SDS. This is confirmed both from DWS and micro imaging. The average drop size obtained from DWS is smaller than the one obtained by micro imaging because DWS is representative of the bulk of emulsion. Micro imaging probes a subpopulation of drops close to the cuvette wall but through drop size distribution gives an idea of the polydispersity (Figure 30).

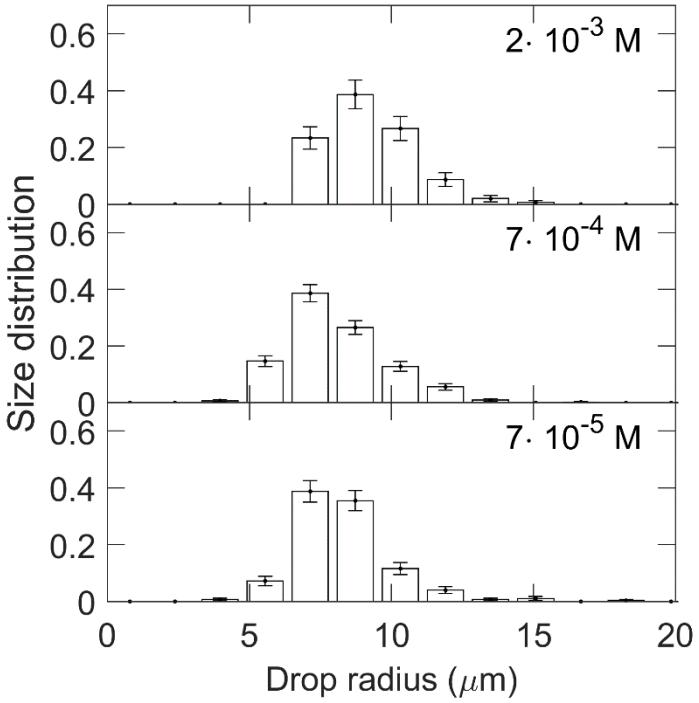

Figure 30 Histograms of the drop radius distribution of emulsions with different SDS concentration aged 15 *days. Figure adapted from* [47].

5.4 MECHANICAL RESPONSE

The relaxation of the DWS correlation function reflects the average response of the emulsion deriving from isolated or collective relaxation processes of droplets. Being a response to a thermal excitation, they could be for example droplet shape deformation or flickering, droplet translations, coalescence between droplets or Ostwald ripening. In Section 5.2 the single droplet's dynamic was observed occurring at the surface as a balance between diffusion in the bulk and relaxation processes of the adsorption layer. This may help to identify what is the dynamic observed by DWS. For emulsions stable for long time it can be ruled out that the dynamic arises from any irreversible process, such as drop-drop coalescence or Ostwald ripening. Flickering of an isolated droplet would be too fast to be detected by DWS in this configuration [44], it could be argued that a collective motion derived from it, could in principle be slower. However, we deem this possibility unlikely. A more plausible explanation can be hypothesized involving local perturbations of the adsorbed layer as a consequence of translation of droplets. Thus, it can be assumed that the decay of DWS correlation functions is represented by the displacement of the centre of mass of the droplets.

Investigating adsorbed layer and emulsions dynamics allows to determine the viscoelastic response of the emulsion. Mechanical modulus of emulsions can be obtained from the mean square displacement of this scattering centres through Equations 18 and 19.

Figure 31 depicts an example of the frequency dependence of elastic and viscous moduli deduced from the mean square displacement $\langle \Delta r^2(\tau) \rangle$ for an emulsion with $[SDS] = 1 \cdot \ 10^{-3} M$ in Regime III). For frequency $\omega > 10 \frac{rad}{s}$ the response is viscous with $G'' \gg G'$, while below this threshold $G'' \sim G'$ means a viscoelastic response [45], [46]. When the viscous modulus $G"$ is dominant, it is roughly proportional to frequency. Near the threshold G' develops a plateau over a small range of frequencies and rises more sharply at higher frequencies until it matches G'' predicting a viscoelastic behaviour in the limit of frequency window reliability.

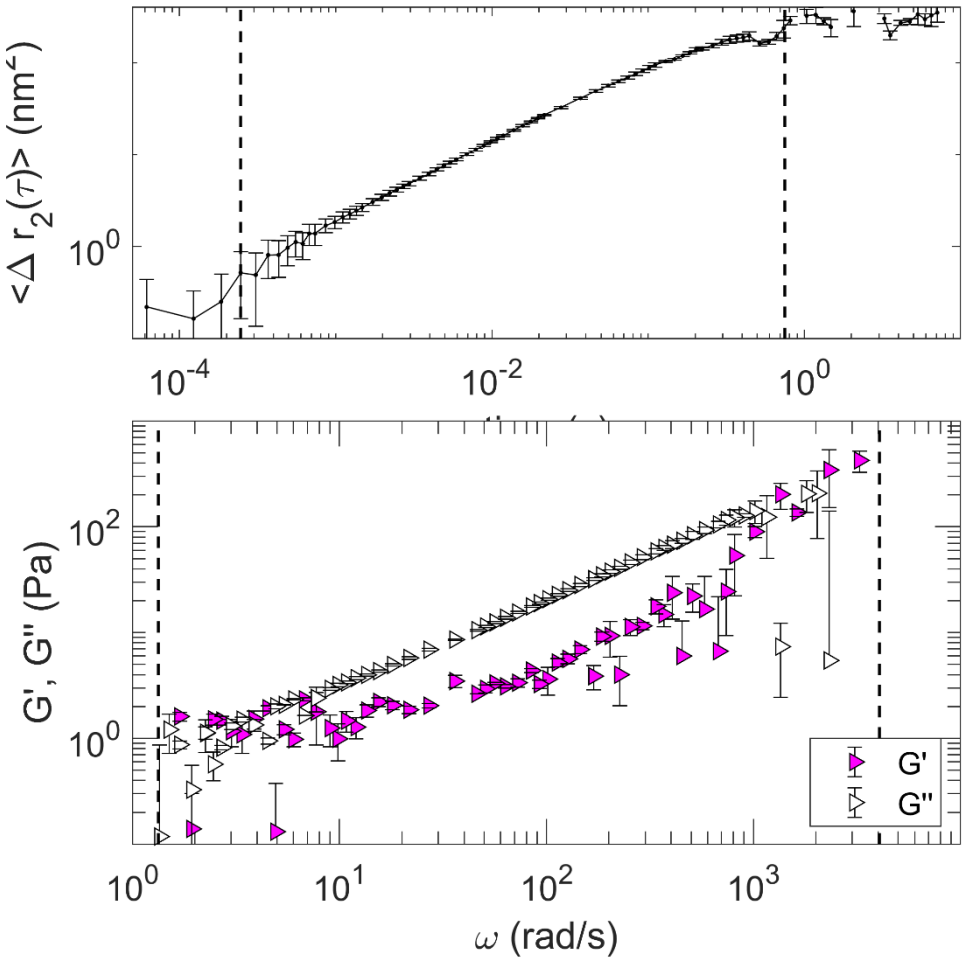

Figure 31 Top) Mean square displacement from Equation 17; Bottom) Elastic modulus G′ (filled symbols) and viscous modulus G″ (empty symbols) as a function of frequency from Equation 19. Data from DWS correlation functions in Transmission on an emulsion with $[SDS] = 1 \cdot 10^{-3} M$ *aged* $20\ days$*. Vertical dashed line set limits for the accuracy determined as explained in Section 2.4.2. Figure adapted from* [47].

All the stable emulsions ($[SDS] > 3 \cdot 10^{-4} M$) show this behaviour with an interesting trend of the shear modulus $|G|$: it grows significantly in Regime II) and follows a power law function of aging time, $|G| \propto t_{age}^{\alpha}$, in Regime III). For the last case the growth of the modulus is shown in Figure 32 for emulsions with different SDS concentration at frequency $\omega = 30{,}100$ and $500\ \frac{rad}{s}$. The power law that describe this dependence from aging has an average value of the exponent $\alpha \simeq 0.20 \pm 0.02$ (Table 2) independent from the concentration of SDS. Since there are no structural changes in emulsions as explained in Section 5.3, the growth of the mechanical modulus with aging may be related to progressive drainage of water inducing slowly increasing of oil drop packing.

On the contrary, at constant aging, the dependence of the dynamics from surfactant concentration shows a peak of the relaxation time, corresponding to a maximum in the bulk shear mechanical modulus quite independent of the frequency. Figure 33 shows τ_B and G'' at different SDS concentration showing a similar trend with a maximum around $[SDS] = 2\ mM$, both quantities in fact are measurement of the correlation functions decay.

Table 2 Values of the exponent α estimated from the power law $|G| \propto t_{age}^{\alpha}$(Figure) at different frequencies and different concentration of SDS for stable emulsions in Regime III).

$[SDS]$	**30 *Hz***	**100 *Hz***	**500 *Hz***
$1 \cdot 10^{-3} M$	$\alpha = 0.22$	$\alpha = 0.20$	$\alpha = 0.26$
$3 \cdot 10^{-3} M$	$\alpha = 0.17$	$\alpha = 0.18$	$\alpha = 0.28$
$5 \cdot 10^{-3} M$	$\alpha = 0.15$	$\alpha = 0.19$	$\alpha = 0.15$

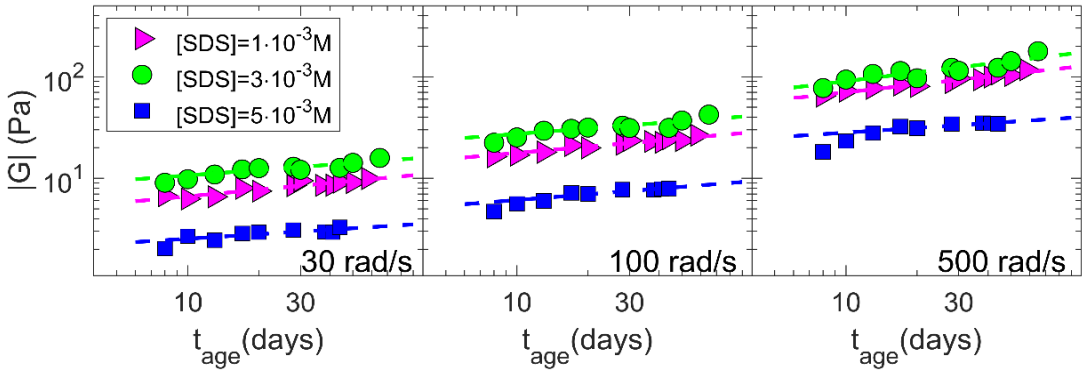

Figure 32 Growth of the mechanical shear modulus $|G|$ at different frequencies described by the power law $|G| \propto t_{age}^{\alpha}$(values of α in Table 2) for stable emulsions at different SDS concentration. Figure adapted from [47].

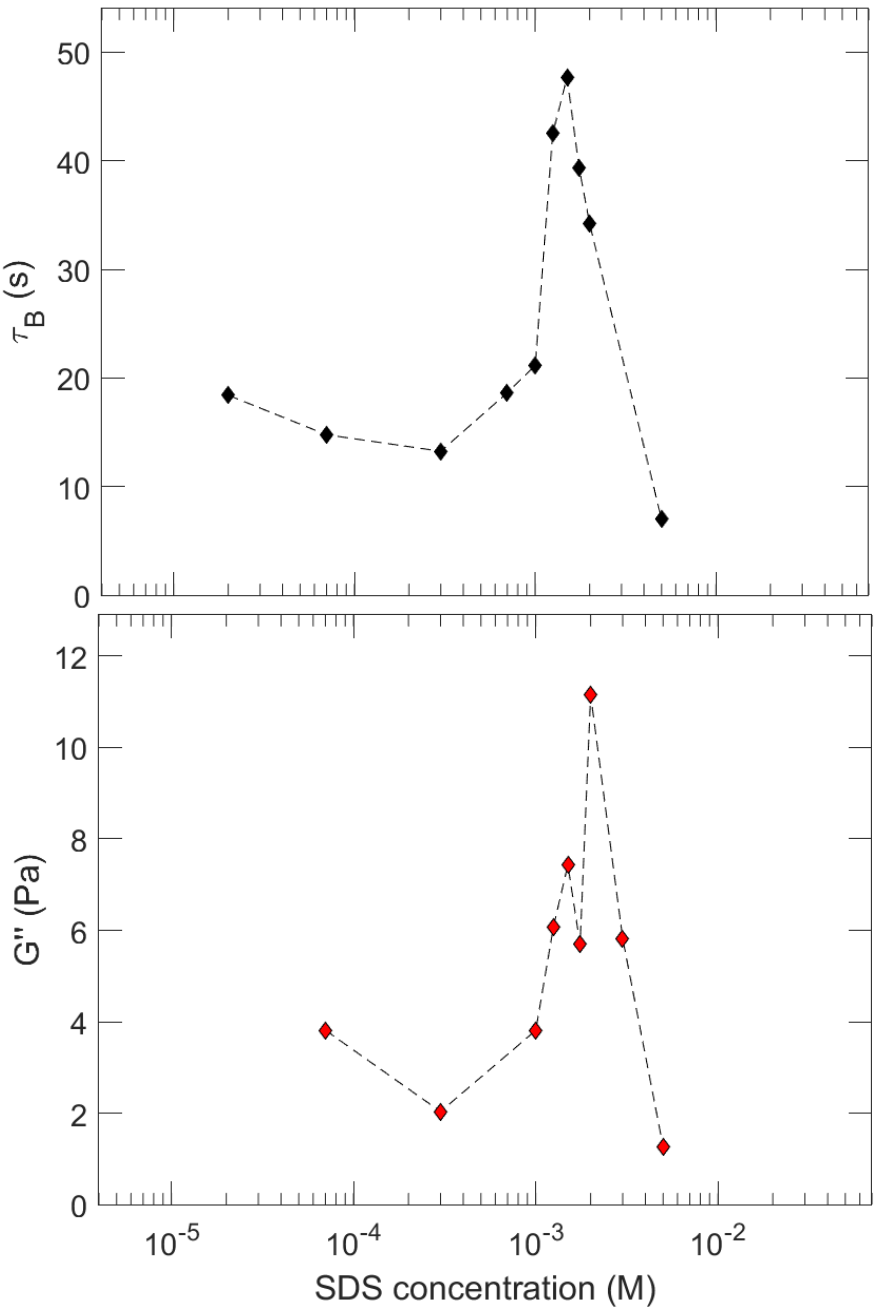

Figure 33 SDS dependence of the DWS relaxation time τ_B (top) and the shear modulus G''at $\omega = 14\ \frac{rad}{s}$ (bottom) at the average age of $11\ days$. Figure adapted from [47].

5.5 RHEOLOGICAL PROPERTIES: FROM DROPLET INTERFACE TO EMULSION

Optical characterization of droplets and emulsions, giving insight on their morphology, dynamics and mechanical response, allows us to discuss the influence that the initial composition has on the final asset, as well as the effects of aging on the properties of the emulsions.

Results obtained by tensiometry of SDS at the water-dodecane interface reported a drop coalescence hindered by SDS molecules coverage also at low adsorption ($[SDS] > 1 \cdot 10^{-6} M$), and Ostwald ripening that has effect only for very tiny droplets in the time window investigated. For the emulsions under study DWS analysis and micro imaging found droplet radius of size $\sim 5 \mu m$ independent from SDS concentration.

Emulsions with $[SDS] > 3 \cdot 10^{-4} M$ are stable for at least $5\, months$, while at less concentration phase separation is observed in about $10\, days$. Dynamic has been investigated for long time aging by DWS: in the first hours (Regime I)) emulsions evolution is dominated by creaming, during the first $10\, days$ (Regime II)) the dynamic evolves and slows down for longer aging (Regime III)). It is assumed that dynamics of less stable emulsions are characterized by irreversible events, e.g. drop coalescence and consequent creaming of the oil drop to the top. Evaluation of the necessary time for the brakeage of these emulsions may be of the order of $T = \left(\frac{N}{R}\right)$ where N is the number of drops per volume and $R \approx \frac{1}{\tau_0 l^{*3}}$ is the volumetric rate of the rearrangement events [17]. From DWS data, it is estimated $R = 10^3 \frac{1}{s\, cm^3}$; considering $2 \cdot 10^9$ drops per cm^3 , T is then equal to $11\, days$ which corresponds to the macroscopic observations of the de-emulsification of emulsions at low SDS content. The results of drop coalescence experiments can be compared with those on emulsion stability by considering in the latter case that SDS initial concentration in the water phase is lower because of the adsorption at the interface.

Dynamics occurring at the droplet interface is a balance between diffusion in the bulk and relaxation processes of the adsorption layer. Investigating adsorbed layer and emulsions dynamics allows to deduce their mechanical properties and in particular their viscous character. Figure 34 compare the SDS dependence of the shear modulus G'' deduced from DWS (depicted in Figure) at $\omega = 14\, rad/sec$ in Regime III) and the dilational viscosity η_{dil} from Drop Shape Tensiometry (depicted in Figure). The close coincidence of the position of the maxima of these quantities validates the hypothesis

of a correlation between mechanical properties of the emulsion on the macro scale and relaxation processes of the adsorption layer. Also in this case, the maximum is observed at smaller SDS concentration for a drop immersed in a solution with respect to an emulsion, where the higher surface available for the adsorption results in impoverishment of the surfactant. The relation found between single drop dilational viscoelasticity and emulsion dynamics can be rationalized by considering the mechanism affecting this dynamic: drop displacements perturb the surfactant layers adsorbed at the drop surfaces, and this perturbation couples to interfacial dilatation and diffusion processes. More explicitly, translation of a drop induces a tangential stress along its interface, which may result in perturbation of the adsorption equilibrium, with gradients of the distribution of surfactant molecules along the drop interface. Return to equilibrium is governed by diffusion processes that recover these gradients, possibly involving both in plane diffusion mechanism (Marangoni flow), but also exchange of surfactant molecules between the interface and the bulk. This latter mechanism also governs the dilational behavior probed by the single drop measurements.

Therefore, we are allowed to conclude that the emulsion dynamics probed by DWS, although mainly related to shear processes, at the single drop level is related to the dilational propertied of the single interface. This is an example of how fundamental local properties determine features on the macroscopic scale which impact on desired functionality and applications.

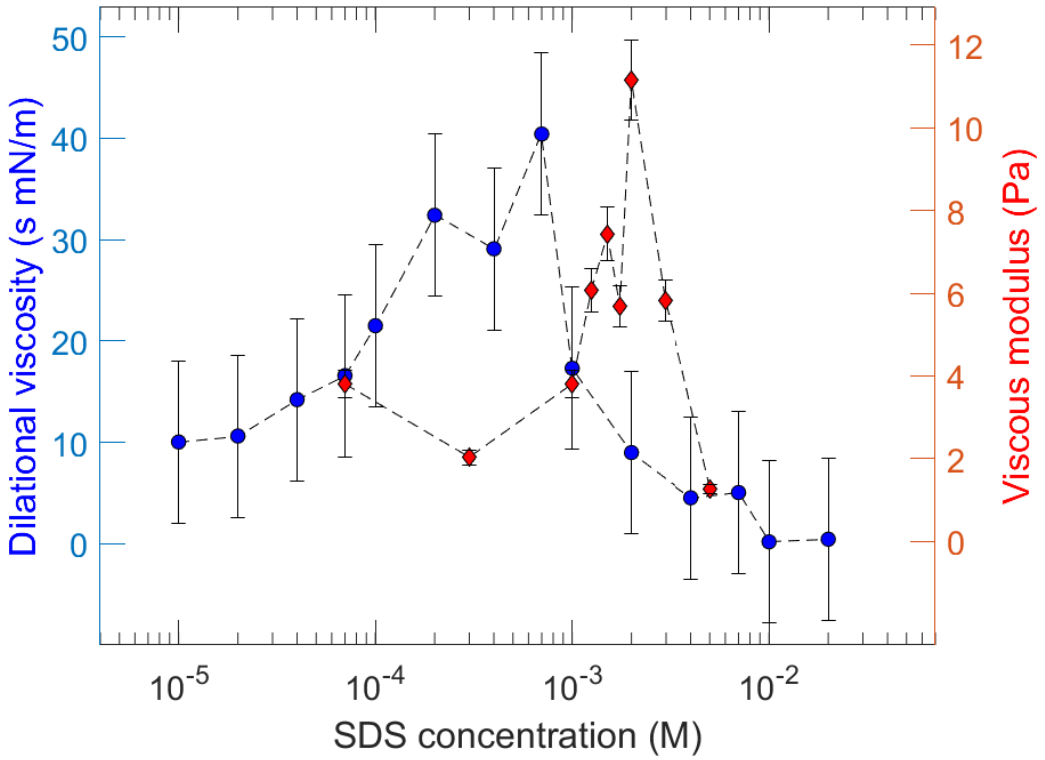

Figure 34 SDS dependence of the dilational viscosity η_{dil} *(blue circles) and the shear modulus* G''*(red diamonds).*

6. CONCLUSIONS

This thesis reports a comprehensive characterization of structure and dynamics from single droplets to emulsions. It was obtained by combining optical techniques on the drop interface adsorption layer with those on whole emulsion. The study of the structure, dynamic and mechanical properties of the single drop was performed by:

- Drop Shape Tensiometry, investigating chemico-physical and mechanical features of the adsorption layer at the liquid-liquid interface (dynamic interfacial tension, surfactant adsorption kinetics and isotherms, and dilational viscoelasticity);

and of emulsions by

- direct imaging of the temporal evolution of the emulsion fraction;
- microscopy digital image processing for comparison and investigation of the evolution of drop size distributions;
- Diffusing Wave Spectroscopy as non-invasive investigation of dynamics, structure and rheological properties, based on time-correlation analysis of coherent light after multiple scattering by the sample.

The combination of these different analysis gave a consistent picture of the factors influencing droplet size distribution, stability and dynamic of the system under study. Emulsions were investigated as a function of compositional parameters and emulsification energy. The emulsification techniques are listed below in order of increasing energy:

- syringe forcing;
- pulsating piston with a device used at AIRBUS Defence and Space in Friedrichshafen and a similar one at the Laboratory of Chemical Technology at Aristotle University of Thessaloniki. These devices were developed to reproduce the “Soft Matter Dynamics” device onboard the ISS dedicated to the study of emulsions;
- rotor-stator homogenizer (Ultraturrax).

Last two emulsification processes apply the energy needed for the formation of stable emulsions with a uniform distribution of droplets size and slowly phase separation.

For the study of long-time stability, the thesis focused on a paradigmatic emulsion formed by dodecane and water stabilized by SDS at low concentration and produced with Ultraturrax.

Surfactant adsorption at the interface between the liquid phases is at the basis of the interpretation of the observed phenomenology. The emerging features have been modelled taking into account the dynamic and structural aspects of droplets adsorption layers obtained by the interpretation of the equilibrium and dynamic interfacial tension data on a single drop. Interesting correlation is found on the dependence as a function of surfactant concentration of dynamics observed on single drop and emulsion. Dilational modulus of the interface of a single drop measured by Drop Shape Tensiometry, DWS relaxation time and viscous modulus strongly depend on the concentration of SDS with a similar trend showing a maximum at SDS concentration well below the CMC. It is inferred that dynamic observed by DWS arises from reversible processes, such as droplet fluctuations, inducing tangential stress at the droplet interfaces which dynamic is connected with the dilational viscoelastic modulus.

Emulsion aging at $[SDS] > 3 \cdot 10^{-4} M$ is differentiated in three regimes: I) the first few hours after emulsion production, dominated by fast creaming and drainage; II) a period lasting for $1\ to\ 10\ days$, where macro evolution of the morphology is not observed but internal dynamics from DWS decelerates as aging proceed; III) a long-time regime where the phenomenology does not change, dynamics and mechanical modulus grow following a power law dependent on aging time. This is explained in terms of progressive packing of emulsion droplets and water drainage. On the contrary, coalescence leads to de-emulsification of emulsion at $[SDS] < 3 \cdot 10^{-4} M$ in $10\ days$.

These results can be useful to clarify the mechanism of action of surfactants in the formulation of stable emulsions based on the chemico-physical features of the liquids and interfaces composing it. Finding the best parameters to obtain stable emulsion with low surfactant content can be of interest for environmental and economic reasons. Future experiments in microgravity, to be performed by the "Soft Matter Dynamics" facility onboard the International Space Station shall provide additional insights.

REFERENCES

[1] L. Hollaway, "Polymers," *Construction Materials: Their Nature and Behaviour, Fourth Edition*. p. 305, 2010.

[2] S. S. Dukhin, N. A. Mishchuk, G. Loglio, L. Liggieri, and R. Miller, "Coalescence coupling with flocculation in dilute emulsions within the primary and/or secondary minimum," *Adv. Colloid Interface Sci.*, vol. 100–102, pp. 47–81, 2003.

[3] P. Taylor, "Ostwald ripening in emulsions: Estimation of solution thermodynamics of the disperse phase," *Adv. Colloid Interface Sci.*, vol. 106, no. 1–3, pp. 261–285, 2003.

[4] J. Weiss, N. Herrmann, and D. J. McClements, "Ostwald ripening of hydrocarbon emulsion droplets in surfactant solutions," *Langmuir*, vol. 15, no. 20, pp. 6652–6657, 1999.

[5] G. Chen and D. Tao, "An experimental study of stability of oil-water emulsion," *Fuel Process. Technol.*, vol. 86, no. 5, pp. 499–508, 2005.

[6] L. Ghaicha, R. M. Leblanc, F. Villamagna, and A. K. Chattopadhyay, "Monolayers of Mixed Surfactants at the Oil-Water Interface, Hydrophobic Interactions, and Stability of Water-in-Oil Emulsions," *Langmuir*, vol. 11, no. 2, pp. 585–590, 1995.

[7] G. Östberg, B. Bergenstähl, and M. Huldén, "Influence of emulsifier on the formation of alkyd emulsions," *Colloids Surfaces A Physicochem. Eng. Asp.*, vol. 94, no. 2–3, pp. 161–171, 1995.

[8] S. V. Verbich, S. S. Dukhin, A. Tarovski, Ø. Holt, Ø. Saether, and J. Sjöblom, "Evaluation of stability ratio in oil-in-water emulsions," *Colloids Surfaces A Physicochem. Eng. Asp.*, vol. 123–124, pp. 209–223, 1997.

[9] S. Llamas *et al.*, "Adsorption of SDS at water/dodecane interface in relation to the oil in water emulsion properties," *Langmuir*, 2018.

[10] C. Maze and G. Burnet, "A non-linear regression method for calculating surface tension and contact angle from the shape of a sessile drop," *Surf. Sci.*, vol. 13, no. 2, pp. 451–470, 1969.

[11] Y. Rotenberg, L. Boruvka, and A. W. Neumann, "Determination of surface tension and contact angle from the shapes of axisymmetric fluid interfaces," *J. Colloid Interface Sci.*, vol. 93, no. 1, pp. 169–183, 1983.

[12] L. Liggieri and A. Passerone, "Automatic technique for measuring the surface tension of liquid metals," *High Temp. Technol.*, vol. 7, no. 2, pp. 82–86, 1989.

[13] F. Ravera, G. Loglio, and V. I. Kovalchuk, "Interfacial dilational rheology by

oscillating bubble/drop methods," *Curr. Opin. Colloid Interface Sci.*, vol. 15, no. 4, pp. 217–228, 2010.

[14] F. Bashforth and J. C. Adams, *An attempt to test the theories of capillary action*. Cambridge University Press, 1883.

[15] D. Georgieva, V. Schmitt, F. Leal-Calderon, and D. Langevin, "On the possible role of surface elasticity in emulsion stability," *Langmuir*, vol. 25, no. 10, pp. 5565–5573, 2009.

[16] G. Loglio, P. Pandolfini, L. Liggieri, A. V. Makievski, and F. Ravera, "Determination of interfacial properties by the pendant drop tensiometry: Optimisation of experimental and calculation procedures," *Bubble Drop Interfaces*, pp. 7–38, 2011.

[17] D. A. Weitz and D. J. Pine, "Diffusing-wave spectroscopy," in *Dynamic Light Scattering: The Method and Some Applications*, W. Brown, Ed. Clarendon Press, 1993.

[18] L. Cristofolini, D. Orsi, and L. Isa, "Characterization of the dynamics of interfaces and of interface-dominated systems via spectroscopy and microscopy techniques," *Curr. Opin. Colloid Interface Sci.*, vol. 37, pp. 13–32, 2018.

[19] M. Sutton *et al.*, "Observation of speckle by diffraction with coherent X-rays," *Nature*, vol. 352, no. 6336, pp. 608–610, Aug. 1991.

[20] A. Z. M. Badruddoza *et al.*, "Diffusing wave spectroscopy (DWS) methods applied to double emulsions," *Curr. Opin. Colloid Interface Sci.*, vol. 37, pp. 74–87, 2018.

[21] R. Höhler, S. Cohen-Addad, and D. J. Durian, "Multiple light scattering as a probe of foams and emulsions," *Curr. Opin. Colloid Interface Sci.*, vol. 19, no. 3, pp. 242–252, 2014.

[22] D. J. Durian, D. A. Weitz, and D. J. Pine, "Multiple light-scattering probes of foam structure and dynamics," *Science.*, vol. 252, no. 5006, pp. 686–688, 1991.

[23] R. Höhler and D. Weaire, "Can liquid foams and emulsions be modeled as packings of soft elastic particles?," *Adv. Colloid Interface Sci.*, vol. 263, pp. 19–37, 2019.

[24] L. Cipelletti, H. Bissig, V. Trappe, P. Ballesta, and S. Mazoyer, "Time-resolved correlation: a new tool for studying temporally heterogeneous dynamics," *J. Phys. Condens. Matter*, vol. 15, no. 1, pp. S257–S262, 2003.

[25] B. J. Berne and R. Pecora, *Dynamic Light Scattering*. New York: Dover, 1976.

[26] K. Schatzel, "Accuracy of photon correlation measurements on nonergodic samples," *Appl. Opt.*, vol. 32, no. 21, p. 3880, 1993.

[27] S. Cohen-Addad and R. Höhler, "Rheology of foams and highly concentrated emulsions," *Curr. Opin. Colloid Interface Sci.*, vol. 19, no. 6, pp. 536–548, 2014.

[28] J. Crassous, "Diffusive wave spectroscopy of a random close packing of spheres," *Eur. Phys. J. E*, vol. 23, no. 2, pp. 145–152, 2007.

[29] W. S. Jodrey and E. M. Tory, "Computer simulation of close random packing of equal spheres," *Phys. Rev. A*, vol. 32, no. 4, pp. 2347–2351, 1985.

[30] J. X. Zhu, D. J. Pine, and D. A. Weitz, "Internal reflection of diffusive light in random media," *Phys. Rev. A*, vol. 44, no. 6, pp. 3948–3959, 1991.

[31] D. J. Pine, D. A. Weitz, J. X. Zhu, and E. Herbolzheimer, "Diffusing-wave spectroscopy: dynamic light scattering in the multiple scattering limit," *J. Phys.*, vol. 51, no. 18, pp. 2101–2127, 1990.

[32] F. C. MacKintosh and S. John, "Diffusing-wave spectroscopy and multiple scattering of light in correlated random media," *Phys. Rev. B*, vol. 40, no. 4, pp. 2383–2406, Aug. 1989.

[33] T. G. Mason, "Estimating the viscoelastic moduli of complex fluids using the generalized Stokes-Einstein equation," *Rheol. Acta*, vol. 39, no. 4, pp. 371–378, 2000.

[34] T. G. Mason and D. A. Weitz, "Optical measurements of frequency-dependent linear viscoelastic moduli of complex fluids," *Phys. Rev. Lett.*, vol. 74, no. 7, pp. 1250–1253, 1995.

[35] D. Orsi *et al.*, "Diffusing wave spectroscopy for investigating emulsions: I. Instrumental aspects," *Colloids Surfaces A Physicochem. Eng. Asp.*, no. July, p. 123574, Jul. 2019.

[36] C. Calabrese, "Development of a Miniaturized Demonstrator for Foam Rheology Microgravity Experiments," 2017. [Online]. Available: http://resolver.tudelft.nl/uuid:5ffb33b5-1a1d-489f-8a43-b19fd1791440.

[37] A. Javadi, N. Mucic, D. Vollhardt, V. B. Fainerman, and R. Miller, "Effects of dodecanol on the adsorption kinetics of SDS at the water-hexane interface," *J. Colloid Interface Sci.*, vol. 351, no. 2, pp. 537–541, 2010.

[38] R. K. Owusu Apenten and Q. H. Zhu, "Interfacial parameters for selected Spans and Tweens at the hydrocarbon-water interface," *Food Hydrocoll.*, vol. 10, no. 1, pp. 27–30, 1996.

[39] Z. Zhu, Y. Wen, J. Yi, Y. Cao, F. Liu, and D. J. McClements, "Comparison of natural and synthetic surfactants at forming and stabilizing nanoemulsions: Tea saponin, Quillaja saponin, and Tween 80," *J. Colloid Interface Sci.*, vol. 536, pp. 80–87, 2019.

[40] E. P. Kalogianni *et al.*, "A multi-probe non-intrusive electrical technique for monitoring emulsification of hexane-in-water with the emulsifier C10E5

soluble in both phases," *Colloids Surfaces A Physicochem. Eng. Asp.*, vol. 354, no. 1–3, pp. 353–363, 2010.

[41] V. B. Fainerman, R. Miller, R. Wüstneck, and A. V. Makievski, "Adsorption isotherm and surface tension equation for a surfactant with changing partial molar area. 1. Ideal surface layer," *J. Phys. Chem.*, vol. 100, no. 18, pp. 7669–7675, 1996.

[42] V. B. Fainerman, S. A. Zholob, E. H. Lucassen-Reynders, and R. Miller, "Comparison of various models describing the adsorption of surfactant molecules capable of interfacial reorientation," *J. Colloid Interface Sci.*, vol. 261, no. 1, pp. 180–183, 2003.

[43] H. B. De Aguiar, M. L. Strader, A. G. F. De Beer, and S. Roke, "Surface structure of sodium dodecyl sulfate surfactant and oil at the oil-in-water droplet liquid/liquid interface: A manifestation of a nonequilibrium surface state," *J. Phys. Chem. B*, vol. 115, no. 12, pp. 2970–2978, 2011.

[44] S. A. Rautu, D. Orsi, L. Di Michele, G. Rowlands, P. Cicuta, and M. S. Turner, "The role of optical projection in the analysis of membrane fluctuations," *Soft Matter*, vol. 13, no. 19, pp. 3480–3483, 2017.

[45] T. G. Mason, "New fundamental concepts in emulsion theology," *Curr. Opin. Colloid Interface Sci.*, vol. 4, no. 3, pp. 231–238, 1999.

[46] T. G. Mason, H. Gang, and D. a. Weitz, "Diffusing-wave-spectroscopy measurements of viscoelasticity of complex fluids," *J. Opt. Soc. Am. A*, vol. 14, no. 1, p. 139, 1997.

[47] F. Salerni, D. Orsi, E. Santini, L. Liggieri, F. Ravera, and L. Cristofolini, "Diffusing Wave Spectroscopy for Investigating Emulsions: II. Characterization of a paradigmatic oil-in-water emulsion," *Colloids Surfaces A Physicochem. Eng. Asp.*, vol. 580, no. March, p. 123724, 2019.